ARTICLES

X-ray structure, symmetry and mechanism of an AMPA-subtype glutamate receptor

Alexander I. Sobolevsky[1], Michael P. Rosconi[1]† & Eric Gouaux[1,2]

Ionotropic glutamate receptors mediate most excitatory neurotransmission in the central nervous system and function by opening a transmembrane ion channel upon binding of glutamate. Despite their crucial role in neurobiology, the architecture and atomic structure of an intact ionotropic glutamate receptor are unknown. Here we report the crystal structure of the α-amino-3-hydroxy-5-methyl-4-isoxazole propionic acid (AMPA)-sensitive, homotetrameric, rat GluA2 receptor at 3.6 Å resolution in complex with a competitive antagonist. The receptor harbours an overall axis of two-fold symmetry with the extracellular domains organized as pairs of local dimers and with the ion channel domain exhibiting four-fold symmetry. A symmetry mismatch between the extracellular and ion channel domains is mediated by two pairs of conformationally distinct subunits, A/C and B/D. Therefore, the stereochemical manner in which the A/C subunits are coupled to the ion channel gate is different from the B/D subunits. Guided by the GluA2 structure and site-directed cysteine mutagenesis, we suggest that GluN1 and GluN2A NMDA (*N*-methyl-D-aspartate) receptors have a similar architecture, with subunits arranged in a 1-2-1-2 pattern. We exploit the GluA2 structure to develop mechanisms of ion channel activation, desensitization and inhibition by non-competitive antagonists and pore blockers.

The development and function of the human brain, and its remarkable capacity for experience-dependent change, hinges on the organization and dynamics of chemical synapses—communication 'contact zones' between neurons. At these specialized sites, chemical transmitters released from presynaptic terminals diffuse across the synaptic cleft and activate receptors localized primarily on the postsynaptic cell[1], thereby transmitting the flow of information from one neuron to another. Glutamate is the predominant chemical transmitter of excitatory synapses in the central nervous system[2,3] and receptors for this ubiquitous neurotransmitter are of two classes: metabotropic and ionotropic[4]. Ionotropic glutamate receptors (iGluRs) are ligand-gated ion channels fundamental to neurotransmission at excitatory synapses and are implicated in nearly all aspects of nervous system development and function[5]. iGluRs are also involved in chronic neurodegenerative conditions, in psychiatric disorders and in acute injury or trauma[6–9].

Comprising the iGluR receptor family are AMPA (GluA1–GluA4), kainate (GluK1–GluK5) and NMDA (GluN1, GluN2A–GluN2D, GluN3A–GluN3B) receptors[10–14]. Whereas NMDA receptors are obligate heterotetramers[14], AMPA and kainate subunits form functional homotetramers[10–12,15], although native receptors are almost exclusively heterotetramers[16–18]. Each subunit has a modular composition[19] and includes a large extracellular amino-terminal domain (ATD)[20] that participates in subtype-specific receptor assembly, trafficking and modulation; a ligand-binding domain (LBD) central to agonist/competitive antagonist binding and to activation gating[21]; a transmembrane domain (TMD) that forms the membrane-spanning ion channel[22]; and a cytoplasmic carboxy-terminal domain involved in receptor localization and regulation[23].

AMPA, kainate and NMDA receptors are related in amino acid sequence yet they are divergent with respect to function[5,24]. Whereas non-NMDA receptors exhibit kinetics of activation, deactivation and desensitization on a millisecond timescale[25], NMDA receptors are slower, with corresponding molecular processes occurring on a timescale of tens to hundreds of milliseconds[26]. Furthermore, AMPA and kainate receptors only demand glutamate for activation, whereas NMDA receptors function as coincidence detectors, requiring membrane depolarization to relieve magnesium block[27] together with binding of glycine[28] and glutamate. AMPA receptors sojourn through multiple sub-conductance states contingent upon agonist concentration[15,29], indicating independent LBDs and a sequential mechanism of activation[30]. AMPA and kainate receptors undergo profound desensitization, whereas NMDA receptors desensitize less profoundly and by way of glycine-dependent and glycine-independent mechanisms[31].

The pharmacology of iGluR family members is distinct. AMPA receptors, for example, are non-competitively antagonized by small molecules binding to the juxta-membrane region[32]. By contrast, the ATDs of NMDA receptors harbour binding sites for polyamines, protons, zinc ions and ifenprodil[26,33]. In AMPA receptors, the LBD possesses binding sites for modulators of receptor desensitization and deactivation[34,35]. All iGluR subtypes, however, possess binding sites for pore blockers within the transmembrane ion channel[36].

Despite divergent functional properties, iGluR family members have a common structural design. Clues to the symmetry and architecture of iGluRs derive from studies of isolated domains, demonstrating that ATDs and LBDs assemble as dimeric entities[34,37–40]; from electron microscopy on intact receptors, showing an overall two-fold symmetry[41,42]; and from amino acid sequence analysis and biophysical studies, indicating a ~4-fold symmetric ion channel[19,43]. Absent from our understanding, however, is an accurate, atomic-resolution description of iGluR architecture and symmetry, a definition of subunit arrangement in homomeric AMPA and heteromeric NMDA receptors[44,45], and proof of the symmetry mismatch between the two-fold symmetric extracellular domains and the presumably four-fold symmetric ion channel[34]. To answer these fundamental questions, we embarked on crystallographic and functional studies of a full-length eukaryotic iGluR.

[1]Vollum Institute, [2]Howard Hughes Medical Institute, Oregon Health and Science University, 3181 SW Sam Jackson Park Road, Portland, Oregon 97239, USA. †Present address: Regeneron Pharmaceuticals, Inc., Protein Chemistry Sciences, 777 Old Saw Mill River Road, Tarrytown, New York 10591, USA.

Crystallization and structure determination

We exploited fluorescence-detection size-exclusion chromatography (FSEC)[46] to discover that the rat GluA2 receptor[10,11], expressed as the unedited[47], 'flip' variant[48], was a promising candidate for structural studies (Supplementary Fig. 3a). We further harnessed FSEC to find that *n*-undecyl-β-D-thiomaltoside, the competitive antagonist ZK200775 (ref. 49) and a modified receptor polypeptide, termed $GluA2_{cryst}$, were the optimal detergent, ligand and protein construct for crystallization trials, respectively (Supplementary Figs 1, 2, 3b–d and 4–6). $GluA2_{cryst}$ binds ^{3}H-AMPA with a dissociation constant (K_d) of 3.5 ± 0.5 nM and yields glutamate-gated currents similar to the wild-type receptor (Supplementary Figs 7 and 8). Crystals of $GluA2_{cryst}$ belong to the *P*1 space group, contain one tetrameric receptor in the unit cell and diffract to 3.6 Å resolution (Supplementary Fig. 9 and Supplementary Table 1).

We solved the $GluA2_{cryst}$ structure by molecular replacement, using the high-resolution structures of the isolated GluA2 ATD[39] and the antagonist-bound form of the isolated GluA2 LBD[38] as search probes. Phases were improved by multidomain non-crystallographic symmetry (NCS) averaging, solvent flattening and histogram matching. The resulting electron density maps were of sufficient clarity to build the transmembrane helices comprising the ion channel domain and the linking polypeptides connecting the LBD to the ion channel and the ATD to the LBD (Supplementary Figs 10–12). The weakest density was observed for the S2–M4 linker connecting the LBD and the M4 transmembrane domain. Residues on the cytoplasmic side of the membrane connecting membrane helices M1 to M2, and M2 to M3, were not visible in electron density maps.

We probed the veracity of the polypeptide trace by preparing selenomethionine (SeMet)-labelled receptor of $GluA2_{cryst}$ and of four methionine point mutants at Leu 542 (M1), Gln 586 (Q/R site, M2)[47], Ile 612 (M3) and Val 800 (M4) and by inspecting the corresponding anomalous difference Fourier maps. We formed crystals with a mercury-labelled variant of ZK200775, measured diffraction data at the Hg L_{III} peak, mapped the antagonist binding site in the LBDs, and found additional mercury binding sites, presumably due to residual methyl mercury chloride (Supplementary Table 1 and Supplementary Figs 13–16). Taken together, the diffraction experiments support the

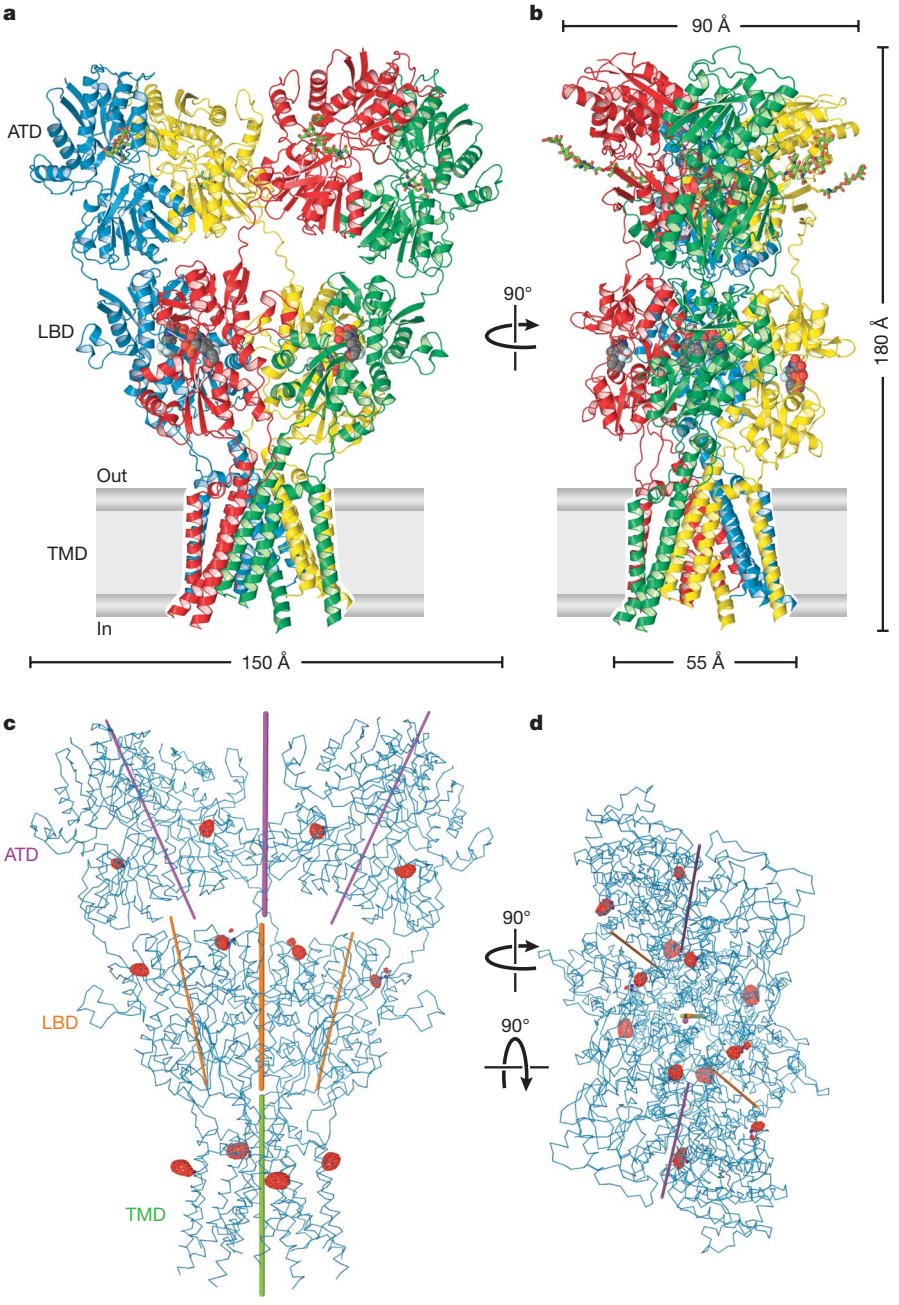

Figure 1 | Architecture of homomeric rat GluA2 receptor. **a**, View of the 'broad' face of the receptor, perpendicular to the overall two-fold axis of molecular symmetry. Each subunit is in a different colour. **b**, View of the 'narrow' face of the receptor. In **a** and **b** competitive antagonist molecules lodged within each LBD clamshell are shown in space-filling representation. **c**, **d**, Axes of symmetry viewed parallel to the membrane (**c**) or from the extracellular 'top' of the receptor, along the overall two-fold axis of symmetry (**d**). Axes of local symmetry for the domains ATD, LBD and TMD are shown in purple, orange and green, respectively. For ATD and LBD, thin lines represent axes of intradimer two-fold symmetry and thick lines represent axes of interdimer two-fold symmetry. For TMD, the thick green line represents the local axis of four-fold symmetry. Red mesh peaks (**c**, **d**) define mercury sites derived from an anomalous difference Fourier map of a $GluA2_{cryst}$ mercury derivative. The contour level is 5.0σ.

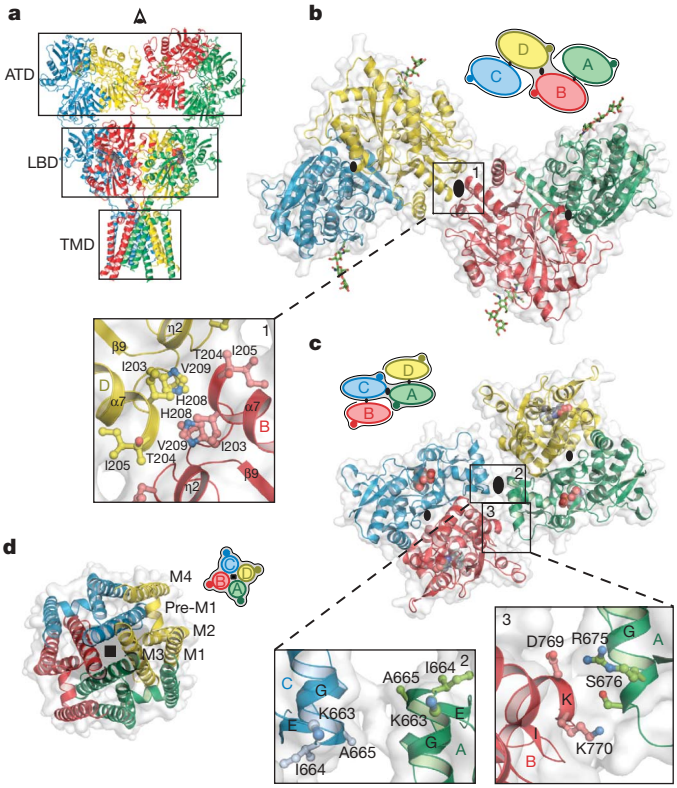

Figure 2 | Domain symmetry and architecture. **a**, $GluA2_{cryst}$ structure viewed perpendicular to the overall two-fold axis. **b–d**, Domain layers viewed from the top of the receptor, parallel to overall two-fold axis. The simple schematics depict the symmetry and arrangement of domains within each layer. **b**, The ATD layer. The boxed region highlights dimer–dimer contacts, with overall two-fold axis (large black oval) in the centre. The local, intradimer two-fold axes of symmetry are shown as smaller black ovals. Subunits B and D are proximal and subunits A and C are distal to the overall two-fold axis, respectively. **c**, The LBD layer with the dimer–dimer contacts on and off the overall two-fold axis shown in panels 2 and 3, respectively. In this layer, subunits A and C are proximal to the overall two-fold axis. **d**, The TMD layer and its four-fold rotational symmetry (black square).

experimental structure, which was refined to good crystallographic statistics and stereochemistry (Supplementary Table 2).

Architecture and symmetry

The GluA2 receptor has a shape like the capital letter 'Y' where the three major domains are arranged in layers (Fig. 1a, b). The TMDs form the ion channel and define the narrow 'base', the ATDs are splayed outward, like diverging prongs, at the 'top' of the Y, and the LBDs, in complex with antagonist molecules, are sandwiched in between the ion channel and ATDs. In this closed, antagonist-bound state of the receptor there are no prominent vestibules or cavities near the ion channel domain and instead the LBD layer rests like a thick slab on top of the ion channel pore (Supplementary Fig. 17).

The symmetry and subunit arrangement of the tetrameric GluA2 receptor is without precedent. The receptor has an overall yet approximate two-fold axis of molecular symmetry oriented perpendicular to the membrane plane (Fig. 1c, d and Supplementary Fig. 16). This two-fold axis of symmetry relates one ATD dimer[39] to another, one LBD dimer[34] to the second, and half of the pore-forming TMDs to the other half. The ion channel domain has an approximate four-fold axis of rotational symmetry (Fig. 1c, d).

Each prong of the receptor Y is defined by an ATD dimer in which the 'local' dimer two-fold axis is oriented ~24° off of the overall two-fold axis (Fig. 1c, d). 'Below' the ATDs are the LBDs, also organized as a pair of dimers in which the local two-fold axes within each dimer are also tipped off the overall two-fold axis of symmetry by ~19° and are thus not aligned with the 'local' ATD two-folds. 'Below' the LBDs the four-fold axis of the ion channel is approximately aligned with the overall two-fold axis of symmetry. The multiple, non-aligned axes of local symmetry, together with the two-fold symmetry of the LBDs and the four-fold symmetry of the ion channel, result in symmetry mismatches between the ATDs, LBDs and TMDs.

Extracellular domains

The ATD, implicated in receptor assembly, trafficking and localization, forms two distinct types of subunit–subunit contacts (Fig. 2). On the one hand, within each ATD 'dimer', there are extensive subunit–subunit contacts (A–B or C–D) that are indistinguishable from the contacts seen in the high-resolution crystal structures of the isolated GluA2 ATDs[39] (Supplementary Fig. 18a). On the other hand there is an interface between ATD dimers (~330 $Å^2$), located on the overall axis of two-fold symmetry, that is mediated by residues on the L2 lobes of the B and D subunits (Fig. 2b). Within the context of the ATD 'layer', we define the B/D and A/C subunits as 'proximal' and 'distal' to the overall two-fold axis of symmetry. The B–D dimer–dimer interface, although small, is observed in the packing of GluA2 ATD dimers in crystals of the isolated ATD[39] (Supplementary Fig. 18b). We suggest that the ATD B–D interface, together with the subunit 'crossover' between the ATD and LBD layers, provides a molecular explanation for the role that the ATD has in the assembly and stability of the tetrameric receptor.

At the LBD layer each agonist binding domain is also a partner in readily identifiable 'dimers' and these dimers, in turn, interact across the overall two-fold axis (Fig. 2c). As a consequence of the subunit crossover between the ATD and LBD layers, the local LBD dimers are formed by the A–D and B–C subunits, with the A and C subunits and the B and D subunits proximal and distal to the overall two-fold axis, respectively. Within a LBD dimer there are multiple contacts between domain 1 of each subunit, recapitulating the interactions seen in the high-resolution crystal structures of the isolated, water-soluble GluA2 LBD[38]. In the

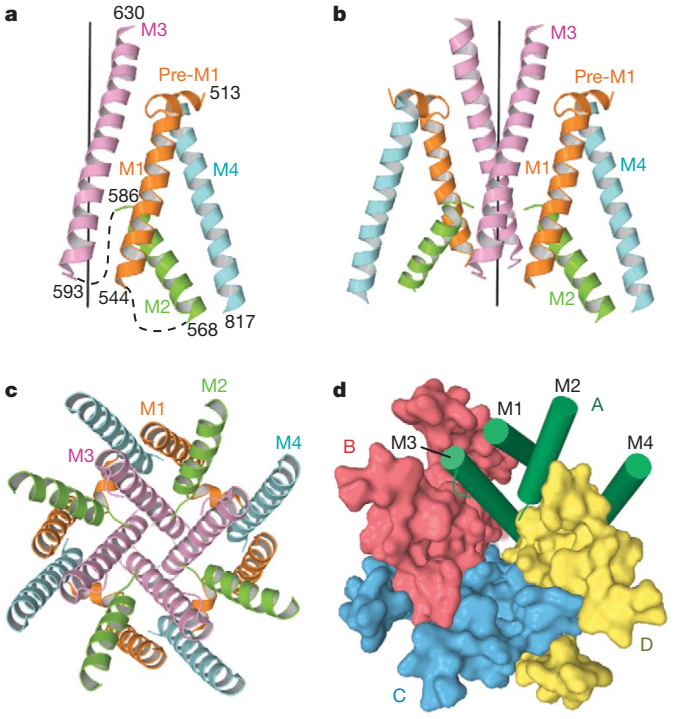

Figure 3 | Transmembrane domain architecture. **a**, **b**, Fold of transmembrane domain for subunit A (**a**) and for subunits A and C (**b**) viewed parallel to the membrane. Transmembrane segments M1 to M4 are depicted in different colours. The 'vertical' black line defines the four-fold symmetry axis. Dashed lines indicate disordered regions. **c**, **d**, TMD viewed parallel to the four-fold axis. **c**, Transmembrane segments are coloured as in panels **a**, **b**. **d**, Surface representation of subunits B to D. For subunit A, the segments M1–M4 are shown as green cylinders.

$GluA2_{cryst}$ structure, which corresponds to an antagonist-bound, non-desensitized state, the domain 1–domain 1 interface is 'intact', as visualized in the wild type[38], the Leu 483 to Tyr mutant or the cyclothiazide[34] and aniracetam-bound[35] structures of the isolated LBD. Domain 2, by contrast, does not participate in significant intersubunit interactions within a LBD dimer, a finding that is also in harmony with high-resolution studies of the isolated LBD[50]. Lodged in the 'clamshell' of each LBD is a bound antagonist, thus proving that the agonist/competitive antagonist binding site is located within and not between subunits.

There is a small (~224 Å^2) interface between LBD dimers, an area consistent with weak dimer–dimer interactions[34,51]. Like the ATD dimer–dimer interface, the LBD dimer interface is located on the overall two-fold axis of symmetry and is composed primarily of residues at the 'bend' between helices F and G, with the α-carbon atoms of residues Lys 663, Ile 664 and Ala 665 of subunits A and C 8–13 Å apart. The relationship between LBD dimers is not perfectly two-fold symmetric, however, and whereas residues at the end of helices G and K of the A and B subunits (Ser 676 and Lys 770) are in van der Waals contact (Cα-Cα distance of 6.1 Å), the equivalent residues in subunits C and D are not in contact (Cα–Cα distance of 9.7 Å).

Transmembrane domain

Viewed from the extracellular side of the membrane down the overall two-fold axis of symmetry, four $GluA2_{cryst}$ subunits arrange their transmembrane domains around an axis of ~4-fold rotational symmetry (Fig. 2d). In accord with topology studies[52,53], each subunit has three transmembrane helices (M1, M3 and M4), a central pore-like helix (M2)[54] and a polypeptide pore-lining loop that is disordered in our electron density maps (Fig. 3a, b). Leading from the LBD, the S1–M1 polypeptide segment adopts an extended conformation until reaching the TMD, at which point the polypeptide forms a ~90° turn and initiates a short helix (pre-M1) oriented nearly parallel to the membrane. The pre-M1 helix acts like a cuff around the 'top' of the ion channel domain, making contacts with carboxyl and amino-terminal ends of helices M3 and M4, respectively. M1 is the first bona fide transmembrane segment and it resides on the exterior of the ion channel domain (Fig. 3c). Within the pore lies the M2 helix, positioned largely on the basis of tube-shaped electron density and the anomalous difference density peak from the SeMet-labelled Gln 586 to Met (Q/R site) mutant. The M3 helices line the inside of the ion channel domain, are ~52 Å in length and, in the present, antagonist bound structure, cross at the level of the pre-M1 cuff helices, near the membrane–aqueous solution boundary, forming a ~12 Å occlusion of the putative ion permeation pathway. Residing on the exterior of the ion channel domain is the M4 helix, connected to the S2 segment of the LBD by two turns of helix and a short extended region of polypeptide. There are extensive subunit–subunit interactions between the transmembrane segments with the M4 segment of one subunit making interactions primarily with the transmembrane domains of an adjacent subunit (Fig. 3d). These interactions provide a molecular basis for the crucial role of the M4 helix in receptor assembly and function[22].

Probing subunit interfaces

Cognisant that the $GluA2_{cryst}$ structure (Fig. 4a) possesses an unorthodox subunit arrangement and molecular symmetry, we tested whether the subunit arrangement and domain–domain contacts in the crystal structure reflect interactions adopted by the receptor in a non-crystalline environment. To accomplish this, we introduced cysteine residues into the three unexplored interfaces at sites that should result in spontaneous disulphide bond formation (Fig. 4b–d). We purified the mutant, tetrameric receptors to homogeneity and probed the extent of spontaneous subunit crosslinking by gel electrophoresis under reducing and non-reducing conditions (Fig. 4e–g and Supplementary Fig. 19).

At the ATD, dimer–dimer, B to D subunit interface, we introduced a cysteine at Val 209 (Fig. 4b). For the wild-type-like receptor, in the presence or absence of reducing agent, the GluA2 subunit migrates at a position consistent with its calculated molecular mass. By contrast, for the Val 209 to Cys mutant, we observe reducing-agent-dependent dimer formation, thus supporting the presence of this dimer–dimer interface in the intact receptor under native conditions (Fig. 4e). In the LBD layer, there are two distinct subunit–subunit interfaces. One

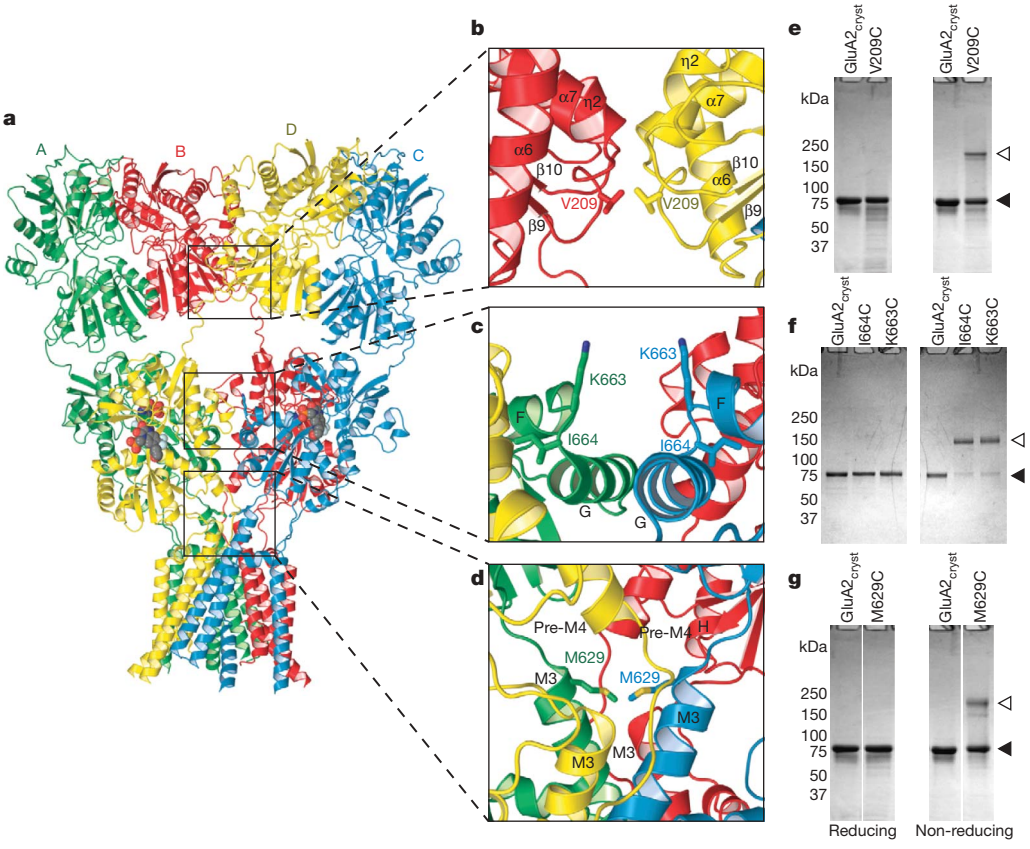

Figure 4 | Probing intersubunit interfaces in GluA2 AMPA receptors. a, Ribbon diagram of the $GluA2_{cryst}$ structure with each subunit in a different colour. **b–d**, Close-up views of intersubunit interfaces between two ATD dimers (**b**), two LBD dimers (**c**) and at the top of the ion channel (**d**). **e–g**, SDS–PAGE analysis of spontaneous crosslinking of cysteines introduced at intersubunit interfaces. Left and right panels illustrate experiments carried out in reducing and non-reducing conditions, respectively. Filled and open triangles indicate positions of monomeric and dimeric bands, respectively.

interface is within a LBD dimer and is formed by extensive contacts between domain 1 of two-fold related subunits, faithfully mirroring the thoroughly documented dimer interface observed in the isolated LBDs of AMPA[34,38,51], kainate[55] and NMDA[56,57] receptors. The second interface, between subunits (A and C) proximal to the overall two-fold axis, is composed of only a handful of intersubunit contacts (Fig. 4c). We therefore tested whether residues in this interface could form inter-dimer disulphide crosslinks. At both Lys 663 and Ile 664 cysteine mutants formed redox-dependent dimers (Fig. 4f), supporting the presence of this interface in the intact receptor. This LBD dimer–dimer interface is also important for agonist-dependent gating because steady-state currents of the Ile 664 to Cys mutant are potentiated ~5-fold after receptor reduction[58] (Supplementary Fig. 20).

The apex of the ion channel domain, defined by the C-terminal ends of M3, provides an important test of the GluA2$_{cryst}$ structure, not only because residues at the end of M3 define the gate of the ion channel in this antagonist-bound state, but also because the end of M3 and the M3–S2 linker span the transition between the four-fold symmetry of the ion channel and the two-fold symmetry of the extracellular domains. In two subunits (A and C), the Met 629 side chains point towards each other and the α-carbons are separated by ~12 Å, whereas the corresponding α-carbon atoms in subunits B and D are 30 Å apart (Fig. 4d). In satisfying agreement with the GluA2$_{cryst}$ structure, we find that cysteines introduced at position 629 form redox-dependent crosslinks (Fig. 4g), consistent with the proximity of Met 629 residues and the structure of the ion channel domain. We may not see complete crosslinking to a dimer position because of the overall two-fold symmetry of the extracellular domains or because some of the cysteine residues may have suffered chemical modification during expression or purification.

We propose that the architecture of kainate receptors is similar to that of the GluA2$_{cryst}$ AMPA receptor based on the remarkable observation that the isolated GluK2 ATD dimer forms a similar dimer-of-dimers arrangement in the crystal lattice, yielding a 'tetrameric' complex[40] like that in the GluA2$_{cryst}$ structure (Supplementary Fig. 21). Superposition of α-carbon atoms for 292 residues per subunit in the structurally conserved regions of GluA2$_{cryst}$ and isolated GluK2 ATD dimer-of-dimers yields a root mean square deviation (r.m.s.d.) of 3.2 Å. This observation, in combination with the fact that LBDs of AMPA and kainate receptors form similar local dimers[55], demonstrates that principles of architecture and symmetry are conserved between AMPA and kainate receptors.

Architecture of NMDA receptors

NMDA receptors are the most complex subfamily of ionotropic glutamate receptors, not only because they are obligate heterotetramers, requiring a glycine-binding GluN1 or GluN3 subunit together with a glutamate binding GluN2 subunit, but also because their ATDs bind ions and molecules that modulate receptor activity[26]. Even though the structure of the GluN1–GluN2A LBD heterodimer is known[56], there is no conclusive experimental knowledge of how subunits are arranged in heterotetrameric NMDA receptors. To determine whether the GluA2$_{cryst}$ structure provides a paradigm for understanding NMDA receptor architecture, we carried out cysteine-directed crosslinking experiments on the rat GluN1–GluN2A NMDA receptor.

Guided by superpositions of the GluN1–GluN2A LBD heterodimer[56] onto the GluA2$_{cryst}$ structure, we designed cysteine substitutions at putative interdimer interfaces. There are three possible arrangements of the GluN1–GluN2A LBD heterodimers within a heterotetrameric receptor and we can distinguish between these models depending on whether redox-dependent crosslinking requires cysteine substitutions in only GluN1, in only GluN2A or in both GluN1 and GluN2A subunits (Supplementary Figs 22 and 23). Remarkably, only a single cysteine substitution in GluN1, at Glu 699, is required to crosslink NMDA receptor subunits at the LBD level (Fig. 5a). Indeed, none of the six cysteine substitutions in GluN2A promoted crosslinking, whereas simultaneous substitutions in both GluN1 and GluN2A resulted in crosslinking similar to

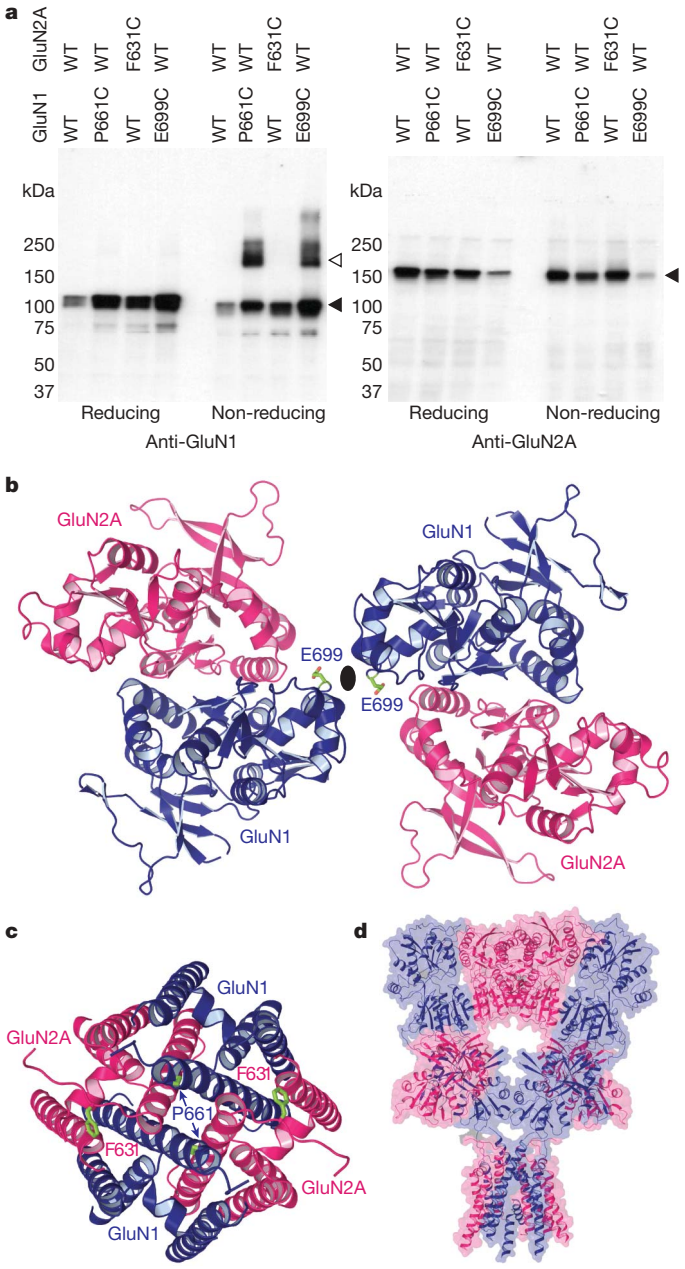

Figure 5 | Subunit arrangement in NMDA receptors. **a**, Western blot analysis of crosslinking of wild-type GluN1–GluN2A (WT) and cysteine-substituted NMDA receptors probed with anti-GluN1 (left) and anti-GluN2A (right) antibodies. Filled and open triangles indicate positions of uncrosslinked monomeric and crosslinked dimeric subunits, respectively. **b**, Model of LBD dimer-of-dimers built by superposing two GluN1–GluN2A dimers[56] on to the GluA2$_{cryst}$ structure, viewed along the axis of overall two-fold symmetry. Residues substituted with cysteines are shown in green. **c**, Model of the NMDA receptor ion channel based on the GluA2$_{cryst}$ structure and viewed along the axis of pseudo-four-fold symmetry. **d**, Simple model of NMDA receptor architecture based on the GluA2$_{cryst}$ structure and using the GluN1–GluN2A LBD heterodimer structure together with the GluA2$_{cryst}$ ATDs and TMDs.

substitutions in GluN1 alone. Within the LBD layer of the NMDA receptor, therefore, we propose that GluN1 and GluN2A subunits form diagonal pairs with the GluN1 subunit proximal to the overall two-fold axis of symmetry (Fig. 5b).

What is the arrangement of NMDA receptors within their TMD? Here we exploit the GluN1 and GluN2A equivalents of GluA2 residue Met 629. Because the GluN1 subunit is proximal to the overall two-fold axis of symmetry at the LBD layer, we predict that the GluN1

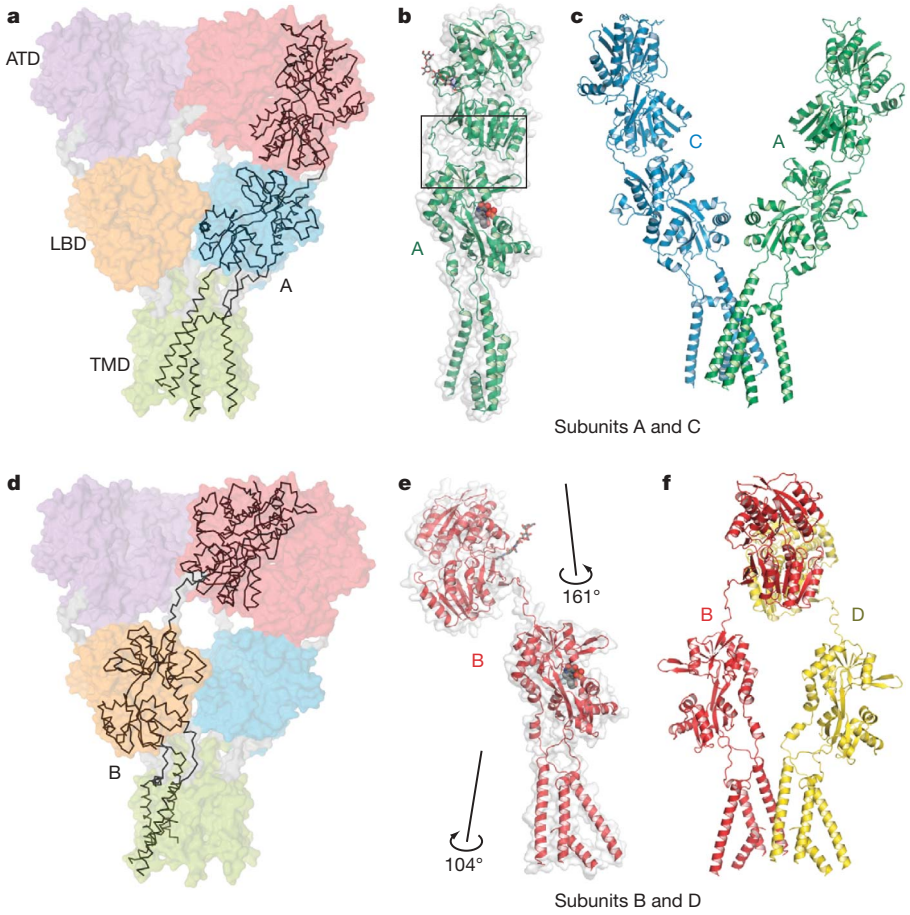

Figure 6 | Subunit non-equivalence and 'domain swapping'. **a**, α-Carbon trace of subunit A and partially transparent solvent-accessible surface of the entire receptor. **b**, Conformation of subunit A. **c**, Position and conformation of subunits A and C in the intact receptor. **d**, α-Carbon trace of subunit B showing 'domain swapping' in going from the ATD to the LBD layers. **e**, Conformation of subunit B. **f**, Position and conformation of subunits B and D in the intact receptor. Note the large differences of the ATD–LBD linkers and ATD–LBD interfaces between the A/C and B/D subunit pairs.

residue, Pro 661, will be proximal to the overall two-fold axis at the TMD layer and that the GluN2A residue, Phe 631, will be too far away to form a crosslink (Fig. 5c). In concordance with this prediction, GluN1(Pro661Cys)–GluN2A(wild type) but not GluN1(wild type)–GluN2A(Phe631Cys) receptors demonstrate redox-dependent crosslinking (Fig. 5a). Even though we have not explored crosslinking of NMDA receptors' ATDs, based on our observation that subunits switch proximity to the overall two-fold axis between the ATD and LBD layers, we predict that the ATDs are assembled as 'local' heterodimers and that NR2 ATDs mediate the dimer–dimer contacts, proximal to an overall two-fold axis of symmetry (Fig. 5d). This arrangement would appropriately position the L2 lobe of the GluN2A ATD to alter receptor structure and function by either modulating ATD dimer–dimer contacts or ATD–LBD interactions, ultimately influencing ion-channel gating via perturbation of the LBD[26,57].

Subunit non-equivalence and domain swapping

There is a remarkable swapping of domains, involved in local dimers between subunits, that is illustrated by tracing neighbouring polypeptide chains through the receptor. Within the ATD layer, subunits A and B interact with each other to form a local ATD dimer (red dimer, Fig. 6a, d). When the polypeptide chains of subunits A and B pass to the LBD layer, however, subunit A forms a LBD dimer with the corresponding domain of subunit D (blue dimer, Fig. 6a), while subunit B associates with subunit C (orange dimer, Fig. 6d). Within the TMD, the transmembrane helices of subunits A and B form extensive contacts with each other as well as with subunits C and D (Fig. 3c, d).

The swapping of extensive local dimer interactions between subunits and the symmetry mismatch between the LBDs and TMDs mean that within this homotetrameric receptor, where each subunit is chemically identical, there are two conformationally different subunit pairs related by the overall axis of two-fold molecular symmetry: subunit A is equivalent to C and subunit B is equivalent to D yet the A/C pair is distinct, in conformation, from the B/D couple (Fig. 6c, f). These differences in conformation can be illustrated by superimposing the LBDs of subunits A and B (Fig. 6b, e), showing the large differences in orientation of the flanking ATDs and TMDs. In subunit A or C, for example, there is a substantial interface between the ATD and LBD (~315 Å^2), whereas in subunit B or D there are no similar contacts (Fig. 6b, e). Another fundamental difference is that the LBD of the B/D subunits is ~6 Å closer to the putative membrane plane than the A/C subunit pair.

The conformational difference between the two types of subunits is defined by polypeptides linking the ATDs, LBDs and TMDs that have the same amino acid sequence but adopt different conformations. These polypeptides also mediate symmetry transitions between domain layers. The symmetry mismatch between the ATDs and the LBDs, characterized by different orientations of their local two-fold axes of symmetry (Fig. 1c, d) and domain swapping (Fig. 6a, d), is mediated by the ATD–S1 linkers (Thr 377–Lys 393). On the one hand, the ATDs of the A and C subunits interact with their LBDs via an ATD–LBD interface (Fig. 6a–c) and the ATD–S1 linkers adopt a more compact conformation. On the other hand, the ATDs of the B and D subunits are suspended between LBD dimers and the ATD–S1 linker nearly spans a LBD dimer, taking on an extended conformation (Fig. 6d–f).

Two-fold to four-fold symmetry transition

On the extracellular side of the membrane, both the ATD dimers and the LBD dimers are arranged with an overall two-fold symmetry. By contrast, the GluA2$_{cryst}$ TMD has four-fold rotational symmetry (Fig. 3c). Where is the two-fold to four-fold symmetry mismatch structurally reconciled? We can answer this question by examining selenium and mercury positions derived from SeMet-labelled receptor and from crystals grown with the mercury-containing antagonist. Selenium sites at Met 629, a residue within the highly conserved 'Glu-Arg-Met-Val' sequence at the end of M3 immediately preceding the S2 segment, clearly show two-fold symmetry (Fig. 7a, b). Mercury

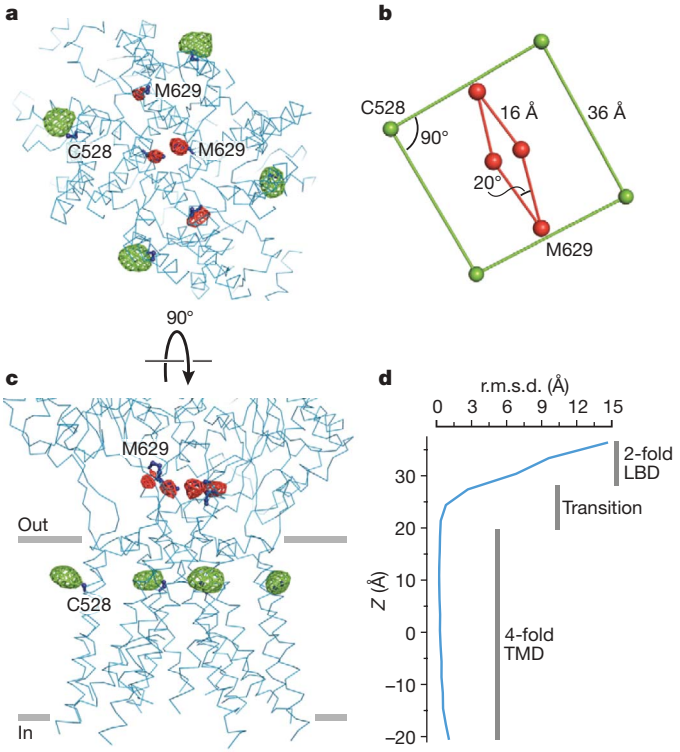

Figure 7 | Two-fold to four-fold symmetry transition. a, Ion channel viewed from the cytoplasm, parallel to the local four-fold axis of symmetry. Mercury (green mesh) and selenium (red mesh) sites, defined by anomalous difference electron density, contoured at 5.0σ and 2.6σ, respectively. **b**, Geometry of the mercury and selenium sites from panel **a**. **c**, View of the TMD perpendicular to its local four-fold axis of molecular symmetry. **d**, Graph showing the r.m.s.d. values of α-carbon positions following transformation of the A subunit on the B subunit by applying the local four-fold axis of symmetry, emphasizing that the two-fold to four-fold symmetry transition occurs between the LBDs and the membrane-embedded TMD. The '*Z*' axis is along the four-fold TMD axis with an origin near the ion channel Gln 586 Q/R site.

sites at Cys 528, near the extracellular end of M1, however, demonstrate unambiguous four-fold symmetry (Fig. 7a, b). By viewing the receptor perpendicular to the overall two-fold axis, and defining the approximate membrane boundary based on residue polarity, we see that Met 629 is just 'outside' of the membrane-spanning region whereas Cys 528 resides within the membrane bilayer. The two-fold to four-fold symmetry transition occurs within this region, a ~10-Å thick slab between the LBDs and TMDs (Fig. 7c).

To define precisely where the transition occurs, we applied the four-fold rotational transformation associated with the TMDs to one of the receptor subunits and calculated the r.m.s.d. of α-carbon atom positions between the superimposed subunits. Where the receptor conforms to four-fold symmetry, the r.m.s.d. values in atom positions are on the order of the coordinate uncertainty. In two-fold symmetric regions, however, the r.m.s.d. values in atom positions are much greater. Thus, by plotting the r.m.s.d. in atom positions as a function of distance along the overall two-fold axis, we can follow the two-fold to four-fold symmetry transition (Fig. 7d). This analysis demonstrates that the transition is abrupt and is located at the boundary of the extracellular leaflet of the membrane bilayer, adjacent to the region of the ion channel domain encircled by the pre-M1 cuff helical segments.

Gating machinery and symmetry mismatch

The symmetry mismatch between the LBDs and the TMDs is resolved by three linking peptides—the S1–M1 (Lys 506–Gly 513), M3–S2 (Val 626–Glu 634) and S2–M4 (Gly 774–Ser 788) linkers—making the transition from the two-fold, parallelogram-like symmetry of

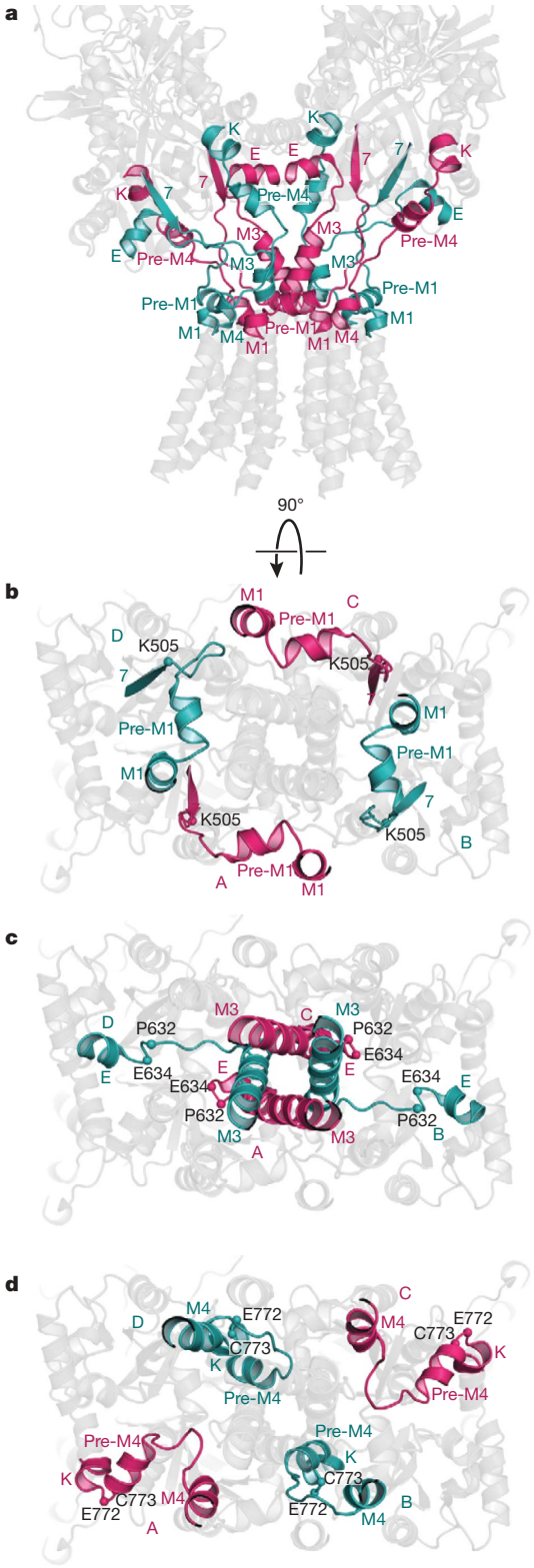

Figure 8 | Gating 'machinery' accommodates symmetry mismatch. a, LBDs and TMDs of $GluA2_{cryst}$ viewed perpendicular to the overall two-fold axis of molecular symmetry. The elements mediating symmetry mismatch between LBDs and TMDs—the S1–M1, M3–S2 and S2–M4 linkers—are coloured pink (subunits A and C) or blue (subunits B or D). **b**–**d**, The elements resolving symmetry mismatch between the LBDs and the TMDs viewed from the cytoplasm, parallel to the ion channel four-fold axis of symmetry. The S1–M1 linkers (**b**), the M3–S2 linkers (**c**) and the S2–M4 linkers (**d**) are shown.

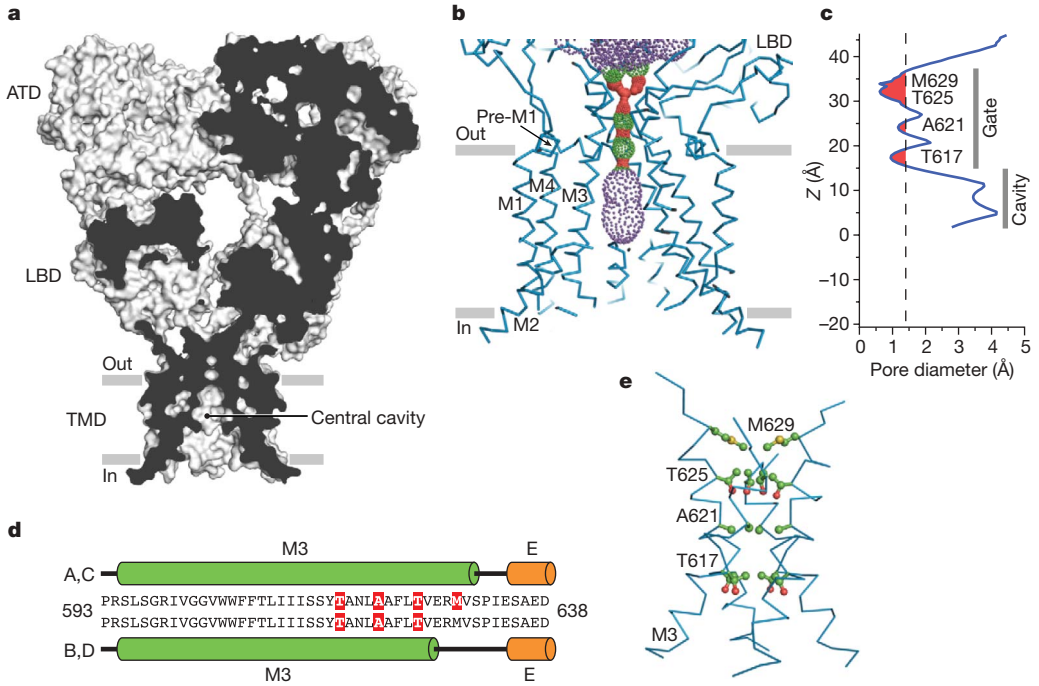

Figure 9 | Closed conformation of the ion channel pore. **a**, Sagittal section of the GluA2$_{cryst}$ receptor illustrates that the occlusion of the putative ion permeation pathway, or the ion channel gate, is located near the extracellular side of the membrane, at the crossing of the M3 helices. **b**, **c**, Surface representation of the ion conduction pathway (**b**) and the pore diameter as a function of distance along the central axis of the channel (**c**) generated using the program HOLE (red < 1.4 Å < green < 2.8 Å < purple). Residues forming the narrowest portions of the ion conduction pathway are indicated. **d**, The A/C and B/D M3 segments adopt distinct conformations at their C termini, proximal to the LBDs. Helical regions are shown as cylinders and coloured green for TMD and orange for LBD. Residues forming the narrowest portions of the ion conduction pathway are highlighted in red. **e**, M3 residues forming the narrowest portion of the ion conduction pathway.

the LBDs to the four-fold symmetric, square geometry of the TMDs (Fig. 8a). Indeed, these are the central elements of the iGluR gating machinery that transform ligand-induced structural changes in the LBD dimers into the movement of the transmembrane domains that opens and closes the central pore of the four-fold symmetric ion channel. In bridging two-fold to four-fold symmetry transition, the peptide segments linking the LBDs and TMDs can be grouped into two pairs that belong to diagonal subunits A/C or B/D; within each group, the linkers adopt approximately similar conformations whereas between the groups the conformations are clearly distinct.

Accommodation of the two-fold to four-fold symmetry mismatch is illustrated by the different conformations of the S1–M1 linkers which, when passing from the β7 strand of the LBD to M1 (TMD), either come from inside (A/C) or outside (B/D) of the 'M1 circle' (Fig. 8b). The M3–S2 linker provides a particularly striking example of how the conformations of the A/C and B/D linking peptides differ. In the A and C subunits, the M3–S2 linker adopts a helical conformation to Met 629 (Fig. 4d). For the B and D subunits, by contrast, the helical conformation is broken at Val 626 and following this residue, the peptide adopts an extended conformation. The difference in main-chain conformation means that the α-carbon atoms of Pro 632 in the A and C subunits are ~27 Å apart whereas the corresponding atoms in the B and D subunits are separated by ~50 Å (Fig. 8c). A third striking illustration is provided by Cys 773, a conserved residue at the end of helix K of the LBD. For Cys 773, in subunits B and D, the α-carbons are 33 Å apart and in the A and C subunits, the span is much larger, 69 Å. To reach the M4 in TMD, which possesses four-fold symmetry and where the distances between the same atom in the A/C and B/D subunits are necessarily the same, the A/C and B/D S2–M4 linkers take on different conformations and different orientations relative to the overall two-fold axis (Fig. 8d).

The ion channel

The four-fold rotationally symmetric GluA2$_{cryst}$ ion channel is shaped like a Mayan temple with a broad cytoplasmic base, ~42 Å on a side, and with a bluntly pointed extracellular 'top'. In the present, competitive antagonist-bound state, the ion channel unambiguously adopts a closed conformation by the crossing of the M3 helices (Fig. 9). The crossing of the helices occurs near the highly conserved Ser-Tyr-Thr-Ala-Asn-Leu-Ala-Ala-Phe (SYTANLAAF) motif, with Thr 617, Ala 621 and Thr 625 occluding the ion channel permeation pathway[22,59]. In the Lurcher mouse[60] there is a substitution of Ala 636 by Thr in the GluD2 subunit, leading to spontaneously opening ion channels[61]. The equivalent residue in GluA2 (Ala 622) participates in close contacts with the M3 helix of a neighbouring subunit, indicating that introduction of bulky residues can directly destabilize the tight helix crossing associated with the resting, closed state of the receptor, leading to constitutively open ion channels. The ion channel permeation pathway is also occluded above the SYTANLAAF motif by a pair of Met 629 residues on the A/C

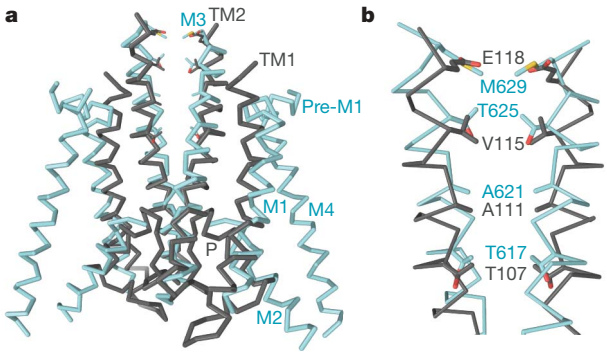

Figure 10 | Closed state conformations of iGluR and K^+ channels are similar. **a**, **b**, Two diagonal subunits (**a**) and their bundle crossing (**b**) in GluA2$_{cryst}$ channel (blue) and KcsA channel[54] (grey) viewed parallel to the membrane. Channels were superimposed by aligning main-chain atoms of the M3 and M1 segments in iGluR with the inner and outer helices in KcsA, respectively. Residues forming the narrowest portions of the ion conduction pathway are shown as stick models.

subunits protruding their side chains towards the centre of the pore. Notably, these methionines are adjacent to the Glu 627–Arg 628 motif that, when mutated, strongly perturbs receptor desensitization[62].

Stimulated by hypotheses[19] and experimental data[43,63] proposing a common architecture for the ion channel pores of iGluRs and K^+ channels, we superimposed the transmembrane domains of $GluA2_{cryst}$ onto the bacterial K^+ channel KcsA[54] (Fig. 10 and Supplementary Fig. 24). Despite the low pairwise identity of ~20% between the aligned amino acid sequences of the rat GluA2 receptor channel and KcsA (Supplementary Fig. 25), the M1, M2 and M3 segments of $GluA2_{cryst}$ overlap remarkably well with structurally equivalent portions of KcsA (Fig. 10a). In fact, superposition of α-carbon atoms for 64 residues per subunit in $GluA2_{cryst}$ and KcsA yields a r.m.s.d. of 2.2 Å. Not included in this comparison was transmembrane segment M4, which is absent in KcsA and bacterial glutamate receptors[64]. In addition to the overall similarity, the structural alignment demonstrates that the occlusion of the ion conductive pathway, that is, the regions of these channels involved in gating and defined by the carboxyl terminal region of M3 in $GluA2_{cryst}$ and TM2 in KcsA, is remarkably similar (Fig. 10b). By contrast, the region of KcsA that confers ion selectivity—the extended Thr-Val-Gly-Tyr-Gly selectivity filter—is completely different in amino acid sequence in iGluRs and is disordered in the $GluA2_{cryst}$ structure, observations consistent with the fact that K^+ channels are highly selective and iGluRs are not.

The pre-M1 cuff helix is oriented nearly parallel to the membrane, at the interface between the membrane and extracellular solution, and is a structural feature that underscores similarities and differences between iGluRs and K^+ channels[65]. Appearing as a 'collar' around the TMD bundle, the pre-M1 helices may restrain the mobility of M3 in the closed state and, by virtue of its connection via the S1–M1 linker to the LBD, promote opening of the ion channel gate upon agonist binding to the LBD. Whereas some K^+ channels have a similar element of structure[65], the length of the helical segment as well as its conformation relative to the ion channel diverge from the $GluA2_{cryst}$ pre-M1 helix. In fact, Pro 520 in the 'elbow' of the $GluA2_{cryst}$ pre-M1 is highly conserved across iGluR subtypes yet is missing in K^+ channels (Supplementary Fig. 25), possibly indicating a distinct role of the pre-M1 element in iGluR structure and gating.

Immediately above the Q/R site, clearly within the transmembrane portion of the ion channel domain, is a central cavity (Fig. 9a) similar to that observed in potassium channels[54]. In the $GluA2_{cryst}$ structure there are conspicuous 'gaps' between the transmembrane domains that result in a portal between the central cavity, within the ion channel, and the membrane environment. We speculate that this portal may be occupied by residues projecting from the transmembrane domains of AMPA receptor auxiliary subunits[66,67], thus providing a mechanism by which auxiliary subunits modulate ion channel properties, such as the extent of block by polyamines[68].

The amino acid sequence and structural relationships between $GluA2_{cryst}$ and K^+ ion channel pores allow us to speculate on the conformation of an iGluR in an open channel state (Supplementary Figs 25 and 26). On the basis of superimposing the ion channels of $GluA2_{cryst}$ and Shaker[65], we suggest that the transmembrane helices of iGluR will bend and splay away from the central axis of the channel, mimicking the iris-like opening of K^+ channels. Although roughly similar in overall nature, the TMD movements during activation gating of iGluRs and K^+ channels may be different in molecular detail[69]. In fact, the residues lining the ion permeation pathway or the amino acids that perturb gating via genetic or chemical modification, together with the types of non-competitive antagonists and channel blockers that bind to the TMD, both in AMPA (Supplementary Fig. 27) and NMDA (Supplementary Fig. 28) receptors, are highly specific to iGluRs, thus providing further evidence of distinction from potassium channels.

Mechanism of activation

The $GluA2_{cryst}$ structure allows us to interpret decades of studies in the context of an intact receptor. Most fundamentally, the $GluA2_{cryst}$

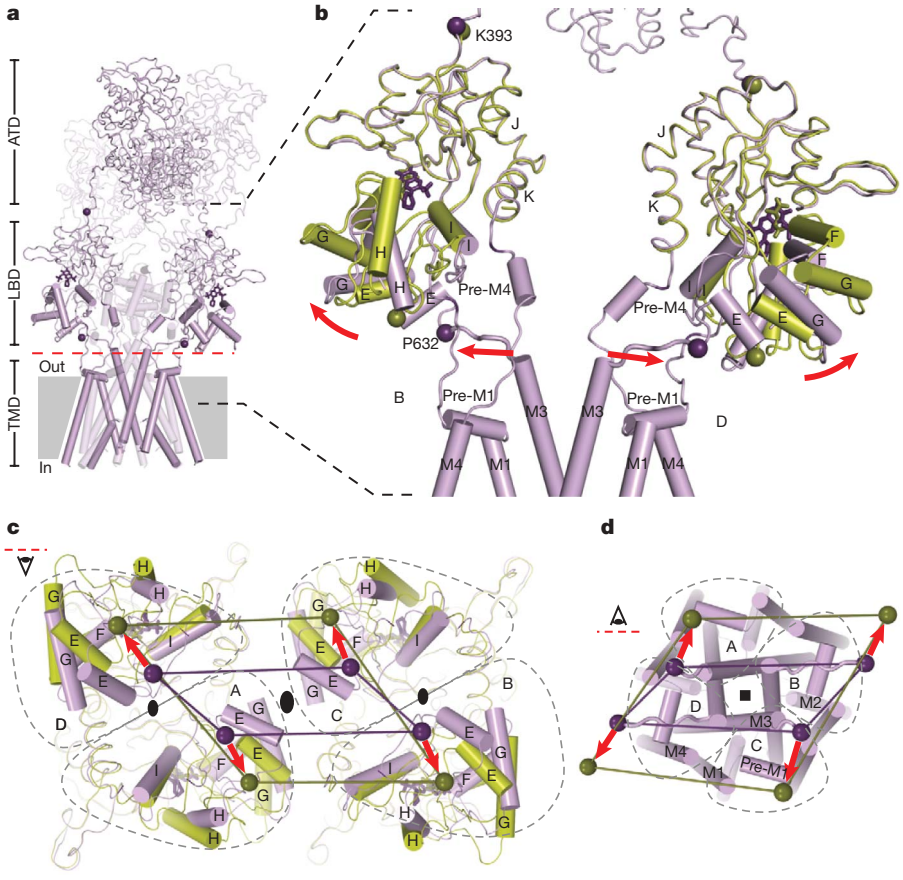

Figure 11 | iGluR activation gating. a, The structure of $GluA2_{cryst}$ with two subunits (A and C) semi-transparent. The red dashed line indicates the interface between LBD and TMD. **b**, Close-up view of the LBD–TMD regions of subunits B and D. The structure of the water-soluble GluA2 LBD (S1S2) crystallized in complex with glutamate[38] has been superimposed, using the D1 domain, on the corresponding region of $GluA2_{cryst}$ and is shown in green. Helical regions of the ion channel as well as parts of the LBD that move upon iGluR activation are shown as cylinders. Purple and green spheres indicate positions of the α-carbons for the residues Lys 393 and Pro 632. Stick models of ZK200775 and glutamate are shown in purple and green, respectively. Red arrows indicate movement during iGluR activation. **c**, **d**, Views of the iGluR tetramer from the interface between LBD and TMD (red dashed line in **a**) on to the LBD along the overall axis of the two-fold symmetry (**c**) and ion channel along the axis of four-fold symmetry (**d**). Grey dashed lines outline borders of the A, B, C and D subunits. Purple and green lines connect Pro 632 α-carbon atoms.

structure proves that agonist binding sites are located within individual subunit 'clamshells' and not between subunits, as is the case with trimeric P2X[70] and pentameric Cys-loop[71] receptors. This architectural principle is consistent with the observations that binding of multiple agonist molecules and subsequent ion channel activation are largely stepwise, sequential processes[15]. Indeed, the independence of LBD function is further supported by the fact that they can be genetically excised and studied as isolated soluble domains[72]. Together, these properties justify exploiting the wealth of structural and biophysical experiments on soluble LBDs of AMPA[38,58,73], kainate[55,74] and NMDA receptors[56,75,76] to illuminate principles of gating in full-length iGluRs.

The $GluA2_{cryst}$ structure is a complex with the high-affinity competitive antagonist ZK200775. Antagonist binding stabilizes the binding domain clamshell in an open conformation (Supplementary Fig. 29)[38] and, in the context of the LBD dimer, places the transmembrane-associated linker regions closest together (Supplementary Fig. 30). The conformation of the LBD trapped by ZK200775, although similar to the *apo* resting state reported for the isolated LBD[38], is nevertheless more open or overextended (Supplementary Fig. 31). Binding of full agonists, such as glutamate, quisqualate or AMPA, results in closure of the clamshell by movement of domain 2 closer to domain 1 by a ~25° rotation (Supplementary Figs 30 and 31)[38,77]. In the context of the water-soluble LBD dimer, closure of both clamshells increases the separation of the regions linking the binding domains to the transmembrane domains by ~20 Å, using the α-carbon of Pro 632 (M3–S2 linker) as a reference (Supplementary Fig. 30). This movement, therefore, 'pulls apart' the M3 helices at the bundle crossing, opens the ion channel, and is the fundamental conformational change, within the binding domains, that transmits the energy associated with agonist binding to the work required to open the ion channel.

Superposition of two 'dimer' structures of the soluble LBD glutamate complex[38] onto the LBDs of the $GluA2_{cryst}$ structure allows us to visualize activation-related movements in the context of the tetrameric receptor (Fig. 11 and Supplementary Fig. 32). Using α-carbon atoms of residues Lys 506, Pro 632 and Cys 773 as reference points for the S1–M1, M3–S2 and S2–M4 linkers, respectively (Supplementary Fig. 33), the most significant movement involves the M3–S2 linker, an observation in agreement with the critical role of the M3 helix in channel gating. As a consequence of the overall two-fold symmetry relating one ligand binding domain dimer to the other, the movements of the M3–S2 linkers are ~2-fold symmetric, that is, there are large conformational changes within dimers and smaller changes between dimers (Fig. 11c, d), consistent with chemical modification studies suggesting a breakdown in the four-fold symmetry of the ion channel upon receptor activation[78]. Augmenting the intradimer motions of this simple model, there is almost certainly a perpendicular component of movement, between LBD dimers, to facilitate opening of the ~4-fold symmetric pore. A component of movement between dimers is supported by the observation that reduction of the Ile 664 disulphide bridge potentiates glutamate-induced GluA2 currents[58,79] (Supplementary Fig. 20).

The differences in position and conformations of the LBD–TMD linkers between the A/C (proximal) and B/D (distal) subunit pairs also mean that the consequences of agonist binding and LBD clamshell closure on the TMD must necessarily be distinct (Fig. 11c, d). Evidence of this distinction can be seen by measuring the minimal distance between a reference residue within the M3–S2 linker, such as Pro 632, and the overall two-fold axis of symmetry, which is approximately coaxial with the four-fold axis of the TMD (Fig. 11c, d). In so doing, we see that the α-carbon of Pro 632 is ~13 Å and 25 Å distal from the two-fold axis for the A/C and the B/D subunits, respectively. Upon agonist binding and LBD closure, we predict that the α-carbons of Pro 632 will move away from the two-fold axis by ~4 Å and 7 Å for the A/C and B/D subunits, respectively. Thus, the extent of conformational movement for the proximal (A/C) and distal (B/D) subunits is substantially different and is greater for the distal (B/D) subunits. We therefore hypothesize that not only will the consequence of agonist binding to ion-channel gating be different for the proximal (A/C) and distal (B/D) subunits, but that the agonist-induced

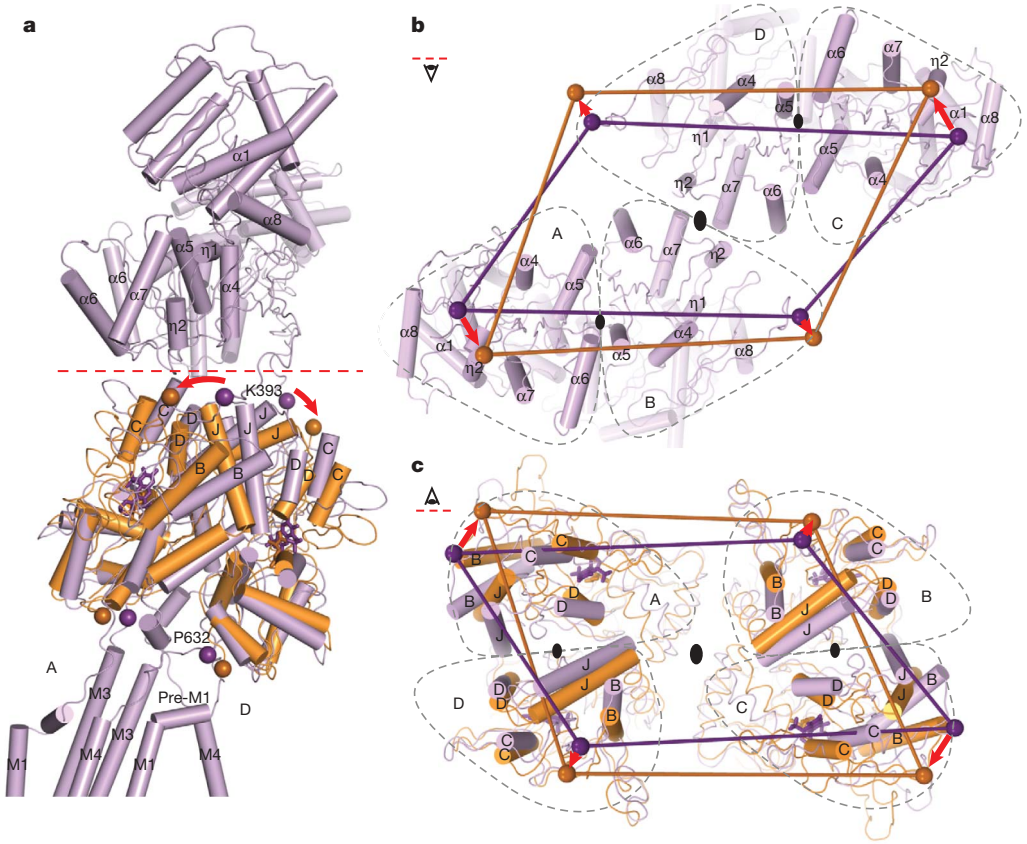

Figure 12 | iGluR desensitization. **a**, Structure of $GluA2_{cryst}$ subunits A and D (purple) with superposed structure of the S729C dimer LBD (orange)[58]. Red dashed line indicates the interface between ATD and LBD. Purple and orange spheres indicate positions of the α-carbons for the residues Lys 393 and Pro 632. Stick models of ZK200775 and glutamate are shown in purple and orange, respectively. Red arrows indicate movement of Lys 393 during GluR desensitization. **b**, **c**, Views on the $GluA2_{cryst}$ tetramer along the overall axis of two-fold symmetry from the interface between ATD and LBD (red dashed line in **a**) looking into the ATD (**b**) and into the LBD (**c**). Grey dashed lines define boundaries of the A, B, C and D subunits.

conformational changes in the distal subunits may be more important to activation gating, simply because the extent of the predicted conformational change is larger. Conversely, we suggest that agonist-induced conformational changes in the proximal subunits may have a comparatively smaller role in activation gating. This explains, at least in part, why in NMDA receptors glycine binding to the GluN1 subunit, which we predict occupies the proximal position in the LBD layer and thus transmits a smaller conformational displacement to the TMD in comparison to the distal subunits, does not result in significant ion channel opening in the absence of glutamate.

Mechanism of desensitization

A hallmark of AMPA and kainate receptors is rapid and profound desensitization, or ion channel closure, after receptor activation[12,48]. The molecular principles of desensitization and the structural relationships between the resting/closed and desensitized states of the ion channel pore are not yet understood for an intact receptor. To address these questions we can exploit the desensitized-like structure of the Ser 729 to Cys (S729C) mutant of the isolated LBD dimer[58]. By superimposing the desensitized-like S729C dimer onto the $GluA2_{cryst}$ structure we find that both D2 lobes of the isolated dimer superimpose well on the corresponding lobes of the tetrameric receptor, even though the isolated domains are bound with glutamate (closed clamshell) and in $GluA2_{cryst}$, the LBDs are 'open' and bound with antagonist. This analysis demonstrates that peptide linkers connecting the LBDs to the TMDs can adopt a similar separation in the antagonist-bound $GluA2_{cryst}$ state and in the glutamate-bound S729C desensitized-like dimer form (Fig. 12 and Supplementary Fig. 30). Desensitization therefore simply involves rupture of the LBD D1–D1 interface and rotation of entire binding domain subunits to allow for the D2 domains and the linkers to the ion channel to adopt a closed-state-like conformation.

In the context of the $GluA2_{cryst}$ structure, rearrangement of D1–D1 LBD interface during desensitization (Fig. 12c) demands movement of the ATDs and the ATD–LBD linkers (Fig. 12b). Upon receptor desensitization, we predict changes in both the distances between and within ATD dimers. These observations provide mechanisms, grounded in three-dimensional structure, by which binding of ions and small molecules to the ATDs of NMDA receptors can modulate receptor function[80]. Ligands alter the conformation of the ATD clamshell and propagate these conformational changes throughout the receptor either directly, through the ATD–LBD linkers, or indirectly, via changes in the ATD dimer–dimer contacts across the overall two-fold axis of symmetry.

Conclusion

The $GluA2_{cryst}$ structure uncovers domain organization and molecular symmetry of iGluRs. Crystallographic and site-directed chemical modification data demonstrate that AMPA, kainate and NMDA receptors have ~2-fold symmetric 'dimeric' extracellular domains, a ~4-fold symmetric ion channel, and a symmetry mismatch that renders diagonally related subunit pairs distinct. In heterotetrameric GluN1/GluN2A NMDA receptors, subunits are positioned in a GluN1–GluN2A–GluN1–GluN2A pattern. Activation gating of iGluRs originates within individual LBDs with agonist binding inducing closure of the clamshell, separation of the transmembrane domain linkers, and opening of the ion channel gate. Desensitization (inactivation) results from rupture of the agonist-bound LBD dimer D1–D1 interface, leading to rigid-body rotation of individual LBD domains within the dimer and allowing for D2 domains, linkers to the ion channel and the ion channel gate to adopt a closed-state-like conformation. Gating can be perturbed at many sites by small molecule inhibitors and modulators, and by auxiliary protein subunits (Supplementary Fig. 34). The underlying architecture and symmetry of iGluRs, as revealed by the $GluA2_{cryst}$ structure, has implications for understanding how these molecules perturb receptor function.

METHODS SUMMARY

The $GluA2_{cryst}$–green fluorescent protein (GFP) fusion (see Methods) was expressed in baculovirus-infected Sf9 insect cells and was purified using metal-affinity chromatography in buffers supplemented with 1.0 mM *n*-dodecyl-β-D-maltoside. Following cleavage by thrombin to remove GFP, the receptor was further purified by size-exclusion chromatography in a buffer supplemented with 1 mM *n*-undecyl-β-D-thiomaltoside and synthetic lipids. Crystallization was performed under paraffin oil, at 4 °C, using a precipitating solution composed of 7–11% (w/v) PEG 20,000, 0.1 M 2-(*N*-morpholino)-ethanesulphonic acid (MES; pH 6.0–6.5) and 300 μM [[3,4-dihydro-7-(4-morpholinyl)-2,3-dioxo-6-(trifluoromethyl)-1(2H)-quinoxalinyl]methyl]phosphonic acid (ZK200775). Selenomethionine-labelled receptor was prepared and crystallized using similar conditions. Diffraction data sets were indexed, integrated and scaled using HKL2000. Initial phase information was obtained by molecular replacement using the isolated N-terminal domains and ligand-binding domains as search probes. The ion channel and interdomain polypeptides were iteratively built using the computer graphics program Coot and the structure was refined using the computer program Phenix. The ion channel functional activity of the $GluA2_{cryst}$ construct was measured by whole-cell or outside-out patch clamp experiments. Ligand binding activity was evaluated by ^{3}H-AMPA saturation and competition assays. NMDA receptor crosslinking experiments were done by transiently transfecting human embryonic kidney tsA 201 cells with wild-type or mutant GluN1 and GluN2A plasmid DNA and analysing oligomeric behaviour of protein on gradient SDS–PAGE gels by western blot analysis. Structure superpositions were done using Superpose (CCP4).

Full Methods and any associated references are available in the online version of the paper at www.nature.com/nature.

Received 25 August; accepted 2 November 2009.
Published online 29 November 2009.

1. Cowan, W. M., Sudhof, T. C. & Stevens, C. F. (eds) *Synapses* (The Johns Hopkins Univ. Press, 2001).
2. Hayashi, T. Effects of sodium glutamate on the nervous system. *Keio J. Med.* **3,** 183–192 (1954).
3. Curtis, D. R., Phillis, J. W. & Watkins, J. C. Chemical excitation of spinal neurons. *Nature* **183,** 611–612 (1959).
4. Sugiyama, H., Ito, I. & Watanabe, M. Glutamate receptor subtypes may be classified into two major categories: A study on *Xenopus* oocytes injected with rat brain mRNA. *Neuron* **3,** 129–132 (1989).
5. Dingledine, R., Borges, K., Bowie, D. & Traynelis, S. F. The glutamate receptor ion channels. *Pharmacol. Rev.* **51,** 7–61 (1999).
6. Jane, D. E., Lodge, D. & Collingridge, G. L. Kainate receptors: Pharmacology, function and therapeutic potential. *Neuropharmacology* **56,** 90–113 (2009).
7. Lipton, S. A. Paradigm shift in neuroprotection by NMDA receptor blockage: memantine and beyond. *Nature Rev. Drug Discov.* **5,** 160–170 (2006).
8. Alt, A., Nisenbaum, E. S., Bleakman, D. & Witkin, J. M. A role for AMPA receptors in mood disorders. *Biochem. Pharmacol.* **71,** 1273–1288 (2006).
9. Labrie, V. & Roder, J. C. The involvement of the NMDA receptor D-serine/glycine site in the pathophysiology and treatment of schizophrenia. *Neurosci. Biobehav. Rev.* doi:10.1016/j.neubiorev.2009.08.002 (18 August 2009).
10. Boulter, J. *et al.* Molecular cloning and functional expression of glutamate receptor subunit genes. *Science* **249,** 1033–1037 (1990).
11. Keinänen, K. *et al.* A family of AMPA-selective glutamate receptors. *Science* **249,** 556–560 (1990).
12. Sommer, B. *et al.* A glutamate receptor channel with high affinity for domoate and kainate. *EMBO J.* **11,** 1651–1656 (1992).
13. Moriyoshi, K. *et al.* Molecular cloning and characterization of the rat NMDA receptor. *Nature* **354,** 31–37 (1991).
14. Monyer, H. *et al.* Heteromeric NMDA receptors: molecular and functional distinction of subtypes. *Science* **256,** 1217–1221 (1992).
15. Rosenmund, C., Stern-Bach, Y. & Stevens, C. F. The tetrameric structure of a glutamate receptor channel. *Science* **280,** 1596–1599 (1998).
16. Lu, W. *et al.* Subunit composition of synaptic AMPA receptors revealed by a single-cell genetic approach. *Neuron* **62,** 254–268 (2009).
17. Mulle, C. *et al.* Subunit composition of kainate receptors in hippocampal interneurons. *Neuron* **28,** 475–484 (2000).
18. Christensen, J. K., Paternain, A. V., Selak, S., Ahring, P. K. & Lerma, J. A mosaic of functional kainate receptors in hippocampal interneurons. *J. Neurosci.* **24,** 8986–8993 (2004).
19. Wo, Z. G. & Oswald, R. E. Unraveling the modular design of glutamate-gated ion channels. *Trends Neurosci.* **18,** 161–168 (1995).
20. O'Hara, P. J. *et al.* The ligand-binding domain in metabotropic glutamate receptors is related to bacterial periplasmic binding proteins. *Neuron* **11,** 41–52 (1993).
21. Stern-Bach, Y. *et al.* Agonist selectivity of glutamate receptors is specified by two domains structurally related to bacterial amino acid-binding proteins. *Neuron* **13,** 1345–1357 (1994).
22. Wollmuth, L. P. & Sobolevsky, A. I. Structure and gating of the glutamate receptor ion channel. *Trends Neurosci.* **27,** 321–328 (2004).

23. Soderling, T. R. & Derkach, V. A. Postsynaptic protein phosphorylation and LTP. *Trends Neurosci.* **23,** 75–80 (2000).
24. Erreger, K., Chen, P. E., Wyllie, D. J. & Traynelis, S. F. Glutamate receptor gating. *Crit. Rev. Neurobiol.* **16,** 187–224 (2004).
25. Hansen, K. B., Yuan, H. & Traynelis, S. F. Structural aspects of AMPA receptor activation, desensitization and deactivation. *Curr. Opin. Neurobiol.* **17,** 281–288 (2007).
26. Paoletti, P. & Neyton, J. NMDA receptor subunits: function and pharmacology. *Curr. Opin. Pharmacol.* **7,** 39–47 (2007).
27. Mayer, M. L., Westbrook, G. L. & Guthrie, P. B. Voltage-dependent block by Mg^{2+} of NMDA responses in spinal cord neurones. *Nature* **309,** 261–263 (1984).
28. Johnson, J. W. & Ascher, P. Glycine potentiates the NMDA response in cultured mouse brain neurons. *Nature* **325,** 529–531 (1987).
29. Smith, T. C. & Howe, J. R. Concentration-dependent substate behavior of native AMPA receptors. *Nature Neurosci.* **3,** 992–997 (2000).
30. Klein, R. M. & Howe, J. R. Effects of the lurcher mutation on GluR1 desensitization and activation kinetics. *J. Neurosci.* **24,** 4941–4951 (2004).
31. Vyklicky, L., Benveniste, M. & Mayer, M. L. Modulation of *N*-methyl-D-aspartic acid receptor desensitization by glycine in mouse cultured hippocampal neurones. *J. Physiol.* **428,** 313–331 (1990).
32. Balannik, V., Menniti, F. S., Paternain, A. V., Lerma, J. & Stern-Bach, Y. Molecular mechanisms of AMPA receptor noncompetitive antagonism. *Neuron* **48,** 279–288 (2005).
33. Mony, L., Kew, J. N., Gunthorpe, M. J. & Paoletti, P. Allosteric modulators of NR2B-containing NMDA receptors: molecular mechanisms and therapeutic potential. *Br. J. Pharmacol.* **157,** 1301–1317 (2009).
34. Sun, Y. *et al.* Mechanism of glutamate receptor desensitization. *Nature* **417,** 245–253 (2002).
35. Jin, R. *et al.* Mechanism of positive allosteric modulators acting on AMPA receptors. *J. Neurosci.* **25,** 9027–9036 (2005).
36. Sobolevsky, A. I. Channel block of glutamate receptors. In *Recent Research Developments in Physiology* Vol. 1, Part I (ed. Pandalai, S. G.) 1–38 (Research Signpost, 2003).
37. Kuusinen, A., Abele, R., Madden, D. R. & Keinänen, K. Oligomerization and ligand-binding properties of the ectodomain of the α-amino-3-hydroxy-5-methyl-4-isoxazole propionic acid receptor subunit GluRD. *J. Biol. Chem.* **274,** 28937–28943 (1999).
38. Armstrong, N. & Gouaux, E. Mechanisms for activation and antagonism of an AMPA-sensitive glutamate receptor: Crystal structures of the GluR2 ligand binding core. *Neuron* **28,** 165–181 (2000).
39. Jin, R. *et al.* Crystal structure and association behavior of the GluR2 amino-terminal domain. *EMBO J.* **28,** 1812–1823 (2009).
40. Kumar, J., Schuck, P., Jin, R. & Mayer, M. L. The N-terminal domain of GluR6-subtype glutamate receptor ion channels. *Nature Struct. Mol. Biol.* **16,** 631–638 (2009).
41. Tichelaar, W., Safferling, M., Keinänen, K., Stark, H. & Madden, D. R. The three-dimensional structure of an ionotropic glutamate receptor reveals a dimer-of-dimers assembly. *J. Mol. Biol.* **344,** 435–442 (2004).
42. Nakagawa, T., Cheng, Y., Ramm, E., Sheng, M. & Walz, T. Structure and different conformational states of native AMPA receptor complexes. *Nature* **433,** 545–549 (2005).
43. Chen, G.-Q., Cui, C., Mayer, M. & Gouaux, E. Functional characterization of a potassium-selective prokaryotic glutamate receptor. *Nature* **402,** 817–821 (1999).
44. Mansour, M., Nagarajan, N., Nehring, R. B., Clements, J. D. & Rosenmund, C. Heteromeric AMPA receptors assemble with a preferred subunit stoichiometry and spatial arrangement. *Neuron* **32,** 841–853 (2001).
45. Schorge, S. & Colquhoun, D. Studies of NMDA receptor function and stoichiometry with truncated and tandem subunits. *J. Neurosci.* **23,** 1151–1158 (2003).
46. Kawate, T. & Gouaux, E. Fluorescence-detection size-exclusion chromatography for precrystallization screening of integral membrane proteins. *Structure* **14,** 673–681 (2006).
47. Sommer, B., Köhler, M., Sprengel, R. & Seeburg, P. H. RNA editing in brain controls a determinant of ion flow in glutamate-gated channels. *Cell* **67,** 11–19 (1991).
48. Sommer, B. *et al.* Flip and flop: A cell-specific functional switch in glutamate-operated channels of the CNS. *Science* **249,** 1580–1585 (1990).
49. Turski, L. *et al.* ZK200775: a phosphonate quinoxalinedione AMPA antagonist for neuroprotection in stroke and trauma. *Proc. Natl Acad. Sci. USA* **95,** 10960–10965 (1998).
50. Mayer, M. L. & Armstrong, N. Structure and function of glutamate receptor ion channels. *Annu. Rev. Physiol.* **66,** 161–181 (2004).
51. Horning, M. & Mayer, M. Regulation of AMPA receptor gating by ligand binding core dimers. *Neuron* **41,** 379–388 (2004).
52. Hollmann, M., Maron, C. & Heinemann, S. N-Glycosylation site tagging suggests a three transmembrane domain topology for the glutamate receptor GluR1. *Neuron* **13,** 1331–1343 (1994).
53. Wo, Z. G. & Oswald, R. E. Transmembrane topology of two kainate receptor subunits revealed by N-glycosylation. *Proc. Natl Acad. Sci. USA* **91,** 7154–7158 (1994).
54. Doyle, D. A. *et al.* The structure of the potassium channel: molecular basis of K^+ conduction and selectivity. *Science* **280,** 69–77 (1998).
55. Weston, M. C., Schuck, P., Ghosal, A., Rosenmund, C. & Mayer, M. L. Conformational restriction blocks glutamate receptor desensitization. *Nature Struct. Mol. Biol.* **13,** 1120–1127 (2006).
56. Furukawa, H., Singh, S. K., Mancusso, R. & Gouaux, E. Subunit arrangement and function in NMDA receptors. *Nature* **438,** 185–192 (2005).
57. Gielen, M. *et al.* Structural rearrangements of NR1/NR2A NMDA receptors during allosteric inhibition. *Neuron* **57,** 80–93 (2008).
58. Armstrong, N., Jasti, J., Beich-Frandsen, M. & Gouaux, E. Measurement of conformational changes accompanying desensitization in an ionotropic glutamate receptor. *Cell* **127,** 85–97 (2006).
59. Chang, H.-R. & Kuo, C.-C. The activation gate and gating mechanism of the NMDA receptor. *J. Neurosci.* **28,** 1546–1556 (2008).
60. Kashiwabuchi, N. *et al.* Impairment of motor coordination, Purkinje cell synapse formation, and cerebellar long-term depression in GluRδ2 mutant mice. *Cell* **81,** 245–252 (1995).
61. Zuo, J. *et al.* Neurodegeneration in Lurcher mice caused by mutation in δ2 glutamate receptor gene. *Nature* **388,** 769–773 (1997).
62. Yelshansky, M. V., Sobolevsky, A. I., Jatzke, C. & Wollmuth, L. P. Block of AMPA receptor desensitization by a point mutation outside the ligand-binding domain. *J. Neurosci.* **24,** 4728–4736 (2004).
63. Panchenko, V. A., Glasser, C. R. & Mayer, M. L. Structural similarities between glutamate receptor channels and K^+ channels examined by scanning mutagenesis. *J. Gen. Physiol.* **117,** 345–360 (2001).
64. Kuner, T., Seeburg, P. H. & Guy, H. R. A common architecture for K^+ channels and ionotropic glutamate receptors? *Trends Neurosci.* **26,** 27–32 (2003).
65. Long, S. B., Campbell, E. B. & MacKinnon, R. Crystal structure of a mammalian voltage-dependent Shaker family K^+ channel. *Science* **309,** 897–903 (2005).
66. Chen, L. *et al.* Stargazin regulates synaptic targeting of AMPA receptors by two distinct mechanisms. *Nature* **408,** 936–943 (2000).
67. Schwenk, J. *et al.* Functional proteomics identify cornichon proteins as auxiliary subunits of AMPA receptors. *Science* **323,** 1313–1319 (2009).
68. Soto, D., Coombs, I. D., Kelly, L., Farrant, M. & Cull-Candy, S. G. Stargazin attenuates intracellular polyamine block of calcium-permeable AMPA receptors. *Nature Neurosci.* **10,** 1260–1267 (2007).
69. Sobolevsky, A. I., Yelshansky, M. V. & Wollmuth, L. P. Different gating mechanisms in glutamate receptor and K+ channels. *J. Neurosci.* **23,** 7559–7568 (2003).
70. Marquez-Klaka, B., Rettinger, J., Bhargava, Y., Eisele, T. & Nicke, A. Identification of an intersubunit cross-link between substituted cysteine residues located in the putative ATP binding site of the $P2X_1$ receptor. *J. Neurosci.* **27,** 1456–1466 (2007).
71. Pedersen, S. E. & Cohen, J. B. D-Turbocurarine binding sites are located at α-γ and α-δ subunit interfaces of the nicotinic acetylcholine receptor. *Proc. Natl Acad. Sci. USA* **87,** 2785–2789 (1990).
72. Kuusinen, A., Arvola, M. & Keinänen, K. Molecular dissection of the agonist binding site of an AMPA receptor. *EMBO J.* **14,** 6327–6332 (1995).
73. Armstrong, N., Sun, Y., Chen, G.-Q. & Gouaux, E. Structure of a glutamate receptor ligand binding core in complex with kainate. *Nature* **395,** 913–917 (1998).
74. Mayer, M. L. Crystal structures of the GluR5 and GluR6 ligand binding cores: molecular mechanisms underlying kainate receptor selectivity. *Neuron* **45,** 539–552 (2005).
75. Inanobe, A., Furukawa, H. & Gouaux, E. Mechanism of partial agonist action at the NR1 subunit of NMDA receptors. *Neuron* **47,** 71–84 (2005).
76. Yao, Y., Harrison, C. B., Freddolino, P. L., Schulten, K. & Mayer, M. L. Molecular mechanism of ligand recognition by NR3 subtype glutamate receptors. *EMBO J.* **27,** 2158–2170 (2008).
77. Jin, R., Horning, M., Mayer, M. L. & Gouaux, E. Mechanism of activation and selectivity in a ligand-gated ion channel: structural and functional studies of GluR2 and quisqualate. *Biochemistry* **41,** 15635–15643 (2002).
78. Sobolevsky, A. I., Yelshansky, M. V. & Wollmuth, L. P. The outer pore of the glutamate receptor channel has 2-fold rotational symmetry. *Neuron* **41,** 367–378 (2004).
79. Plested, A. J. & Mayer, M. L. AMPA receptor ligand binding domain mobility revealed by functional cross linking. *J. Neurosci.* **29,** 11912–11923 (2009).
80. Gielen, M., Siegler Retchless, B., Mony, L., Johnson, J. W. & Paoletti, P. Mechanism of differential control of NMDA receptor activity by NR2 subunits. *Nature* **459,** 703–707 (2009).

Supplementary Information is linked to the online version of the paper at www.nature.com/nature.

Acknowledgements We thank the personnel at beamlines 5.0.2, 8.2.1 and 8.2.2 of the Advanced Light Source and at beamline 24-ID-E of the Advanced Photon Source. We also thank T. Homrichhausen for help with cloning and FSEC screening; L. Vaskalis for assistance with illustrations; and Gouaux laboratory members for discussion. M.P.R. was supported by an individual NIH National Research Service Award. This work was supported by the NIH. E.G. is an investigator with the Howard Hughes Medical Institute.

Author Contributions All authors contributed to writing the manuscript.

Author Information Coordinates and structure factors for $GluA2_{cryst}$ and the GluA2 ligand-binding core complex bound with glutamate, LY404187 and ZK200775 have been deposited with the Protein Data Bank under codes 3KG2 and 3KGC respectively. Reprints and permissions information is available at www.nature.com/reprints. Correspondence and requests for materials should be addressed to E.G. (gouauxe@ohsu.edu).

METHODS

Construct optimization and expression. The full-length rat GluA2i (flip) (NP_058957) subunit (also known as GluRBi or GluR2i)[11,81], including the native signal peptide, was subcloned into the pFastBac1 vector for baculovirus expression in Sf9 insect cells using standard methods. For fluorescence detection, size-exclusion chromatography analysis (FSEC)[46] and for small- or large-scale purification, coding sequences for a thrombin cleavage site (Gly-Leu-Val-Pro-Arg-Gly), enhanced green fluorescent protein (eGFP)[82] and an octa-histidine tag were introduced at the C terminus of each receptor construct. To improve crystallization behaviour of the GluA2 receptor, 36 residues were removed from the C terminus, 6 residues (Leu 378, Thr 379, Leu 381, Pro 382, Ser 383 and Gly 384; numbering according to the mature polypeptide sequence) were deleted from the N-terminal domain (ATD)–ligand binding domain (LBD) polypeptide linker, three of four predicted *N*-linked glycosylation sites were knocked out (Asn 235 to Glu; Asn 385 to Asp, and Asn 392 to Gln) and four residues in loop 1 of the LBD were substituted by alanine (Lys 410 to Ala, Glu 413 to Ala, Met 414 to Ala and Glu 416 to Ala). Point mutations of Arg 586 to Gln (Q/R site)[47] and Cys 589 to Ala were introduced to stabilize the tetrameric state of the receptor and to reduce nonspecific aggregation and disulphide bond formation, respectively. All constructs were screened by FSEC before large-scale expression experiments and crystallization trials. Together, these modifications yielded the construct, called $GluA2_{cryst}$, used in the crystallographic studies described here (see Supplementary Figs 1 and 2).

Purification. Infected Sf9 insect cells were harvested 72–96 h after infection and collected by a low-speed centrifugation step (6,000*g*, 10 min). Cells were disrupted using either an Avestin EmulsiFlex-C5 (two passes at 5,000–15,000 p.s.i.) or a Misonix Sonicator 3000 (18 × 15 s, power level 7) in a buffer containing 150 mM NaCl, 20 mM Tris-HCl pH 8.0, 0.8 μM aprotinin, 2 μg ml^{-1} leupeptin, 2 mM pepstatin A and 1 mM phenylmethysulphonyl fluoride (25 ml buffer/1 l Sf9 cell culture). The homogenate was clarified using a Sorval centrifuge (8,000 r.p.m., 15 min) and crude membranes were collected by ultracentrifugation (Ti45 rotor, 40,000 r.p.m., 1 h). The membranes were mechanically homogenized and subsequently solubilized for 2 h in a buffer containing 150 mM NaCl, 20 mM Tris-HCl pH 8.0 and 40 mM $C_{12}M$ (*n*-dodecyl-β-D-maltopyranoside; 0.2 g of $C_{12}M$ per 1 g membranes). Insoluble material was removed by ultracentrifugation (Ti45 rotor, 40,000 r.p.m., 40 min) and cobalt-charged metal ion affinity resin was added to the supernatant. After binding for 12–18 h, the receptor was eluted by application of buffer supplemented with 250 mM imidazole. Following thrombin digestion (1:200 mass ratio of receptor to thrombin) and concentration, the receptor containing solution was loaded onto a size-exclusion chromatography (SEC) column equilibrated in a buffer composed of 150 mM NaCl, 20 mM Tris-HCl pH 8.0, 1 mM *n*-undecyl-β-D-thiomaltopyranoside (C_{11}Thio), and 0.01 mg ml^{-1} lipid: 3:1:1 POPC:POPE:POPG (1-palmitoyl-2-oleoyl-sn-glycero-3-phosphocholine:1-palmitoyl-2-oleoyl-sn-glycero-3-phosphoethanolamine: 1-palmitoyl-2-oleoyl-sn-glycero-3-[phospho-rac-(1-glycerol)]). Peak fractions were pooled and concentrated to ~2 mg ml^{-1} for crystallization experiments. All steps were performed at 4 °C unless otherwise noted. Analysis of the purified receptor by gel electrophoresis and tryptophan FSEC is illustrated in Supplementary Fig. 6.

Crystallization and cryoprotection. Crystallization of the rat GluA2 receptor involved multiple steps of construct modification and crystal growth optimization. In the beginning, the full-length, wild-type receptor did not yield crystals, even though the purified protein was chemically homogeneous and tetrameric in subunit stoichiometry. The first crystals, which diffracted to ~40 Å, were obtained from a construct where we introduced point mutations of Arg 586 to Gln and Cys 589 to Ala and also removed 36 residues from the C terminus. Inclusion of synthetic lipids as well as a 4-residue deletion in the ATD–LBD linker increased the diffraction limit to ~16 Å. The knockout of three out of four predicted *N*-linked glycosylation sites improved the diffraction limit to ~8 Å. Additional removal of two residues from the ATD–LBD linker, optimization of the detergent (C_{11}Thio) and ligand (ZK200775) for crystallization allowed further improvement of diffraction to 4 Å resolution. Finally, alanine substitutions in loop 1 of the LBD, continued optimization of the cryoprotection conditions and crystallization under paraffin oil allowed us to break the 4 Å diffraction limit barrier and measure crystallographic data with reasonable statistics to Bragg spacings of 3.6 Å (Supplementary Table 1).

At present, the most well ordered crystals of the $GluA2_{cryst}$ construct grow at 4 °C in a sitting-drop configuration under paraffin oil at 4 °C. Before crystallization experiments, 0.3 mM ZK200775 or 0.3 mM ZK200775 and 0.3 mM LY404187[83] were added to the $GluA2_{cryst}$ protein solution, which in turn was subjected to ultracentrifugation (Ti100 rotor, 40,000 r.p.m., 40 min, 4 °C). The receptor solution was then mixed with a crystallization buffer composed of 7–11% PEG 20,000 and 0.1 M MES pH 6.0–6.5 at receptor to crystallization buffer ratio of 2:1. Crystals of the receptor appeared after 5–30 days. Cryoprotection was carried out at 4 °C by serial transfer into buffers containing increasing concentrations of glycerol, up to a maximum concentration of 30% (v/v), and then plunged into liquid nitrogen.

Measurement of complete data sets was complicated by the fact that the crystals are radiation sensitive and belong to the space group *P*1, with one GluA2 tetramer per asymmetric unit. The crystals have a diffraction limit of 3.5 Å and a variable mosaic spread from 0.2° to 1.5°. The unit cell dimensions are $a = 91$ Å, $b = 110$ Å, $c = 161$ Å and $\alpha = 85°$, $\beta = 85°$, $\gamma = 79°$, yielding a Matthews coefficient (V_M)[84] of ~4.3 Å^3 Da^{-1}.

Structure determination. X-ray diffraction data sets were collected using synchrotron radiation at the Advanced Light Source (Lawrence Berkeley Laboratory; beamline 5.0.2) and were indexed, integrated and scaled using HKL2000[85]. The structure was solved by molecular replacement using the computer program Phaser[86] and search probes composed of the rat GluA2 N-terminal domain (ATD; Protein Data Bank (PDB) code 3H5V)[39] and the DNQX-bound S1S2 ligand binding domain (PDB code 1FTL)[38]. Electron density for the ion channel and ATD-S1S2 and S1S2-channel linkers that emerged from this solution was used as a guide for building the corresponding regions of the model. The structure of the full-length $GluA2_{cryst}$ was iteratively built and refined using the computer graphics program Coot[87] and Phenix[88], respectively (Supplementary Table 2). The four subunits in the tetrameric receptor structure contain $GluA2_{cryst}$ residues 10 to 817, *N*-linked carbohydrates at Asn 349, and antagonist (ZK200775) molecules in the S1S2 ligand binding pockets. Because of weak electron density for Thr 568 to Phe 584 (helical region of M2), these residues were modelled as alanines. Regions lacking electron density and presumably disordered—residues Arg 545 to Ser 567 (M1–M2 loop), Gln 587 to Ser 592 (non-helical region of M2) and Ser 818 to Gly 832 (C terminus)—were excluded from the final $GluA2_{cryst}$ model.

Electrophysiology and ^{3}H-AMPA binding experiments. The DNA encoding the wild-type GluA2i or $GluA2_{cryst}$ receptors were introduced into a plasmid for expression in eukaryotic cells[11] that was engineered to produce GFP via a downstream internal ribosome entry site[43]. Human embryonic kidney tsA 201 cells grown on glass coverslips in 35-mm dishes were transiently transfected with 1–5 μg of plasmid DNA using Lipofectamine 2000 Reagent (Invitrogen). Recordings were made 24 to 48 h after transfection at room temperature. Currents from whole cells or from outside-out patches, typically held at a –60 mV potential, were recorded using an Axopatch 200B amplifier (Axon Instruments), filtered at 5 kHz and digitized at 10 kHz using HEKA Pulse software (HEKA Elektronik). The external solution contained (in mM): 140 NaCl, 2.4 KCl, 4 $CaCl_2$, 4 $MgCl_2$, 10 HEPES pH 7.3 and 10 glucose; 10 mM NaCl and 10 mM sucrose were added to the extracellular activating solution containing 1 mM L-glutamate. The internal solution contained (in mM): 150 CsCl, 10 NaCl, 10 EGTA, 20 HEPES pH 7.3. Rapid solution exchange was achieved with a two-barrel theta glass pipette controlled by a piezoelectric translator; junction currents were used to estimate speed of solution exchange after recordings. Data analysis was performed using Origin.

Binding experiments with ^{3}H-AMPA were performed following the previously published protocol[89].

Cysteine crosslinking and western blots. Single cysteine substitutions were introduced using conventional PCR-based methods. Constructs were verified by sequencing over the entire length of the iGluR coding region. The parent $GluA2_{cryst}$ or single cysteine substituted constructs in the pFastBac1 vector were expressed in Sf9 insect cells and purified as described above. About 5 μg of protein was subjected to denaturing conditions by addition of 6× SDS sample buffer containing 300 mM Tris-H:Cl (pH 6.8), 12% SDS, 0.6% bromophenol blue and 60% glycerol in the absence (non-reducing condition) or presence (reducing condition) of 100 mM dithiothreitol (DTT). The protein samples were then run on a 4–15% gradient SDS–PAGE gel and protein bands were visualized by Coomassie blue staining.

For NMDA receptor crosslinking experiments, DNA encoding wild-type rat GluN1a (EDL93606) and GluN2A (NP_036705) subunits were introduced into plasmids for expression in eukaryotic cells. The same amounts of wild-type or mutant GluN1 and GluN2A plasmid DNA (1–5 μg) mixed together and Lipofectamine 2000 Reagent (Invitrogen) were used to transiently transfect human embryonic kidney tsA 201 cells. Cells were harvested 24–48 h after transfection and solubilized for 1 h in PBS supplemented with 40 mM $C_{12}M$ (*n*-dodecyl-β-D-maltopyranoside), 0.8 μM aprotinin, 2 μg ml^{-1} leupeptin, 2 mM pepstatin A and 1 mM phenylmethysulphonyl fluoride. Crude solubilized material was clarified by ultracentrifugation (Ti100 rotor, 40,000 r.p.m., 40 min, 4 °C) and then run on a 4–15% gradient SDS–PAGE gel either in the absence (non-reducing condition) or presence (reducing condition) of 100 mM DTT. Protein bands were transferred to the Hybond-ECL nitrocellulose membranes (Amersham Biosciences) using Trans-Blot electrophoretic transfer cell (Bio-Rad). The membranes were blocked for 1 h at room temperature in TBST (150 mM NaCl,

10 mM Tris-HCl pH 7.6, 0.1% Tween-20) containing 5% non-fat milk and 1% BSA and then incubated for 1 h with either mouse anti-NMDAR1 monoclonal (Millipore, MAB1586) or rabbit anti-NMDAR2A polyclonal (Millipore, AB1555P) antibodies. After four 15-min washes with TBST, the membranes were incubated for 1 h at room temperature with either sheep anti-mouse (GE Healthcare, NA931V) or donkey anti-rabbit (GE Healthcare, NA934V) antibodies conjugated to horseradish peroxidase. Then the membranes were washed again four times for 15 min with TBST and immunoreactivity was visualized using the ECL detection kit (Amersham Biosciences).

Structure superpositions. The structures were superimposed using the CCP4 program Superpose. The ATD dimer-of-dimers from $GluA2_{cryst}$ (ABCD subunits) and ATD dimer-of-dimers represented by crystal packing of the isolated GluK2 ATD[40] (ABA′B′ subunits) were superposed based on α-carbon atoms for 292 residues per subunit in the structurally conserved regions (overall sequence identity of the regions, 25.5%): residues 4–14, 17–31, 34–93, 102–109, 111–131, 140–159, 171–259, 273–293, 320–341 and 351–375 for $GluA2_{cryst}$ and 3–13, 20–34, 42–101, 113–120, 125–145, 154–173, 180–268, 286–306, 325–346 and 357–381 for GluK2, respectively. The ion channels of $GluA2_{cryst}$ (ABCD subunits) and KcsA (ADCB subunits) were superposed based on α-carbon atoms for 64 residues per subunit in the structurally conserved regions (overall sequence identity of the regions, 20%): residues 522–544, 575–584 and 595–625 for $GluA2_{cryst}$ and 29–51, 61–70 and 85–115 for KcsA, respectively. The ion channels of Shaker and KcsA were superposed based on α-carbon atoms of the P-loop region (residues 358–375 in Shaker and 63–80 in KcsA, respectively) yielding the r.m.s.d. of 0.7 Å.

81. Hollmann, M., O'Shea-Greenfield, A., Rogers, S. W. & Heinemann, S. Cloning by functional expression of a member of the glutamate receptor family. *Nature* **342,** 643–648 (1989).
82. Cormack, B. P., Valdivia, R. H. & Falkow, S. FACS-optimized mutants of the green fluorescent protein (GFP). *Gene* **173,** 33–38 (1996).
83. Miu, P. *et al.* Novel AMPA receptor potentiators LY392098 and LY404187: effects on recombinant human AMPA receptors *in vitro*. *Neuropharm.* **40,** 976–983 (2001).
84. Matthews, B. W. Solvent content of protein crystals. *J. Mol. Biol.* **33,** 491–497 (1968).
85. Otwinowski, Z. & Minor, W. Processing of X-ray diffraction data collected in oscillation mode. *Methods Enzymol.* **276,** 307–326 (1997).
86. McCoy, A. J. Solving structures of protein complexes by molecular replacement with Phaser. *Acta Crystallogr. D.* **63,** 32–41 (2007).
87. Emsley, P. & Cowtan, K. Coot: model-building tools for molecular graphics. *Acta Crystallogr. D.* **60,** 2126–2132 (2004).
88. Adams, P. D. *et al.* PHENIX: building new software for automated crystallographic structure determination. *Acta Crystallogr. D.* **58,** 1948–1954 (2002).
89. Chen, G. Q. & Gouaux, E. Overexpression of a glutamate receptor (GluR2) ligand binding domain in *Escherichia coli*: Application of a novel protein folding screen. *Proc. Natl Acad. Sci. USA* **94,** 13431–13436 (1997).